

1 **R-loop homeostasis and cancer mutagenesis promoted by** 2 **the DNA cytosine deaminase APOBEC3B**

3
4
5 Jennifer L. McCann^{1-4,#}, Agnese Cristini^{5,#}, Emily K. Law^{1-4,##}, Seo Yun Lee^{6,##}, Michael
6 Tellier⁵, Michael A. Carpenter¹⁻⁴, Chiara Beghè⁵, Jae Jin Kim⁶, Matthew C. Jarvis²⁻⁴,
7 Bojana Stefanovska²⁻⁴, Nuri A. Temiz^{2,7}, Erik N. Bergstrom⁸⁻¹⁰, Daniel J. Salamango²⁻⁴,
8 Margaret R. Brown²⁻⁴, Shona Murphy⁵, Ludmil B. Alexandrov⁸⁻¹⁰, Kyle M. Miller^{6,11},
9 Natalia Gromak^{5,*} & Reuben S. Harris^{1-4,*}

10
11 ¹ Howard Hughes Medical Institute, University of Minnesota, Minneapolis, Minnesota,
12 USA, 55455

13 ² Masonic Cancer Center, University of Minnesota, Minneapolis, Minnesota, USA,
14 55455

15 ³ Institute for Molecular Virology, University of Minnesota, Minneapolis, Minnesota, USA,
16 55455

17 ⁴ Department of Biochemistry, Molecular Biology and Biophysics, University of
18 Minnesota, Minneapolis, Minnesota, USA, 55455

19 ⁵ Sir William Dunn School of Pathology, University of Oxford, South Parks Road, Oxford,
20 UK, OX1 3RE

21 ⁶ Department of Molecular Biosciences, University of Texas at Austin, Austin, Texas,
22 USA, 78712

23 ⁷ Institute for Health Informatics, University of Minnesota, Minneapolis, MN, USA, 55455

24 ⁸ Department of Cellular and Molecular Medicine, UC San Diego, La Jolla, California,
25 USA, 92093

26 ⁹ Department of Bioengineering, UC San Diego, La Jolla, California, USA, 92093

27 ¹⁰ Moores Cancer Center, UC San Diego, La Jolla, CA, 92037, USA

28 ¹¹ Livestrong Cancer Institutes, Dell Medical School, University of Texas at Austin,
29 Austin, Texas, USA, 78712

30 # Equal primary contributions; ## Equal secondary contributions

31 * Correspondence: natalia.gromak@path.ox.ac.uk and rsh@umn.edu

32
33 Running Title: APOBEC3B in R-loop biology and mutagenesis

34
35 Manuscript Information: Abstract 149 words; Article including Refs & Legends 60,000
36 characters; Figs. 1-8; Supplementary Information: Methods; Tables S1-2; Figs. S1-6

37 **Abstract**

38 The single-stranded DNA cytosine-to-uracil deaminase APOBEC3B is an antiviral
39 protein implicated in cancer. However, its substrates in cells are not fully delineated.
40 Here, APOBEC3B proteomics reveal interactions with a surprising number of R-loop
41 factors. Biochemical experiments show APOBEC3B binding to R-loops in human cells
42 and *in vitro*. Genetic experiments demonstrate R-loop increases in cells lacking
43 APOBEC3B and decreases in cells overexpressing APOBEC3B. Genome-wide
44 analyses show major changes in the overall landscape of physiological and stimulus-
45 induced R-loops with thousands of differentially altered regions as well as binding of
46 APOBEC3B to many of these sites. APOBEC3 mutagenesis impacts overexpressed
47 genes and splice factor mutant tumors preferentially, and APOBEC3-attributed *kataegis*
48 are enriched in RTCW consistent with APOBEC3B deamination. Taken together with
49 the fact that APOBEC3B binds single-stranded DNA and RNA and preferentially
50 deaminates DNA, these results support a mechanism in which APOBEC3B mediates R-
51 loop homeostasis and contributes to R-loop mutagenesis in cancer.

52

53 **Key words**

54 APOBEC mutation signature; APOBEC3B; Cancer mutagenesis; DNA damage; DNA
55 deamination; *Kataegis*; R-loop homeostasis; R-loop mutagenesis; RNA/DNA hybrids

56

57 **Highlights**

58 * Unbiased proteomics link antiviral APOBEC3B to R-loop regulation

59 * Systematic alterations of APOBEC3B levels trigger corresponding changes in R-loops

60 * APOBEC3B binds R-loops in living cells and *in vitro*

61 * Bioinformatics analyses support an R-loop deamination and mutation model

62

63 **Introduction**

64 The APOBEC3 family of single-stranded (ss)DNA cytosine deaminases are critical
65 players in the overall innate immune response to viral infection (reviewed by refs.^{1,2}).
66 Popularized initially by potent HIV-1 restriction activity³⁻⁶, the seven human APOBEC3
67 enzymes collectively elicit activity against a broad number of DNA-based viruses
68 including retroviruses (HIV-1, HTLV-1), hepadnaviruses (HBV), papillomaviruses (HPV),
69 parvoviruses (AAV), polyomaviruses (JC and BKPyV), and herpesviruses (EBV, HSV-1)
70 (reviewed by refs.^{1,2}). An important biochemical feature of this family of enzymes is an
71 intrinsic preference for different nucleobases immediately 5' of target cytosines⁷⁻¹¹. For
72 example, APOBEC3B (A3B) and APOBEC3A (A3A) preferentially deaminate cytosines
73 in 5'TC motifs and the related antibody gene diversification enzyme AID targets 5'AC
74 and 5'GC motifs.

75 In addition to beneficial functions in innate and adaptive immunity, multiple DNA
76 cytosine deaminases have detrimental roles in cancer mutagenesis (reviewed by
77 refs.^{1,12-17}). Misprocessing of AID-catalyzed deamination events in antibody gene
78 variable and switch regions can result in DNA breaks and chromosomal translocations
79 in B cell malignancies (reviewed by ref.¹⁷). Off-target deamination of other genes also
80 occurs at lower frequencies and the resulting mutations may contribute to B cell lineage-
81 derived leukemias and lymphomas^{18,19}. In comparison, large-scale tumor sequencing
82 projects have reported an APOBEC mutation signature in a wide variety of cancer types

83 including those derived from breast, lung, head/neck, cervix, and bladder tissues (see
84 recent pan-cancer analysis²⁰ and reviews above). In cancer, the APOBEC mutation
85 signature is defined as C-to-T transitions and C-to-G transversions in 5'TCA and 5'TCT
86 motifs to help distinguish from other mutational processes²¹⁻²⁵. Recent estimates
87 indicate that APOBEC enzymes are the second most prevalent mutation-generating
88 process in human cancer following clock-like mutagenesis which is attributed to
89 ageing²⁰.

90 Despite extensive documentation of the APOBEC mutation signature in cancer,
91 the precise molecular mechanisms governing this mutational process are still unclear.
92 One challenge is the possibility that at least two enzymes, A3B and A3A, combine in
93 different ways to generate the overall signature (*e.g.*, refs.^{21-23,26-28}). However, a few
94 mechanistic insights have still been inferred from the physical characteristics of
95 genomes with, for instance, APOBEC mutations associating with chromosomal DNA
96 replication and specifically with C-to-U deamination events in the lagging strand
97 template²⁹⁻³⁴. Other genomic features and processes with exposed ssDNA may be
98 similarly prone to APOBEC mutagenesis such as single-stranded loop regions of DNA
99 hairpins^{35,36} and ssDNA tracts in recombination and repair reactions, which sometimes
100 manifest clusters of strand-coordinated APOBEC3-attributed mutations (*aka. kataegis*;
101 *e.g.*, refs.^{25,35,37}). Together, these studies have indicated a passive diffusion mechanism
102 in which simple expression of A3B and/or A3A leads to random encounters with any
103 exposed ssDNA followed in some instances by processive local deamination.

104 Another potential substrate for APOBEC enzymes is ssDNA exposed by R-loop
105 formation. R-loops occur when nascent RNA re-anneals to the transcribed DNA strand,

106 creating a three-stranded structure containing an RNA/DNA hybrid and a displaced non-
107 transcribed ssDNA strand (reviewed by refs.³⁸⁻⁴⁰). R-loops are critical for the specialized
108 mechanism of AID-catalyzed antibody gene hypermutation and class switch
109 recombination in B lymphocytes (reviewed by refs.^{41,42}). R-loops also represent a
110 prominent source of genome instability associated with human disease, including
111 cancer (e.g., refs.⁴³⁻⁴⁵; reviewed by refs.^{39,40,46-51}). However, evidence linking APOBEC
112 enzymes to R-loop-associated mutation and genome instability is presently lacking. A
113 potential clue came from recent studies showing a mismatch repair-dependent synthetic
114 lethal interaction between A3B activity and uracil excision repair disruption⁵². This report
115 suggested that the toxic lesions may represent U/G mispairs, which are unlikely to arise
116 through replication but may be created by transcription-associated processes, such as
117 C-to-U deamination within a R-loop.

118 A3B is strongly implicated in cancer mutagenesis based on several criteria
119 including nuclear localization, overexpression in tumors, upregulation by cancer-causing
120 viruses such as HPV, and associations with clinical outcomes (reviewed by refs.^{1,12-14}).
121 To gain deeper insights into the pathological role of A3B in cancer mutagenesis, an
122 unbiased affinity purification and mass spectrometry (AP-MS) approach was used to
123 identify A3B-interacting proteins. Two dozen proteins were recovered in biologically-
124 independent experiments, and 60% of the resulting high-confidence interactors had
125 been reported previously as R-loop-associated factors in RNA/DNA hybrid AP-MS
126 experiments⁵³. A comprehensive series of genetic, cell biology, biochemistry, genomic,
127 and bioinformatic studies was therefore undertaken to investigate the relationship
128 between A3B and R-loops. Surprisingly, the results indicated that A3B functions in R-

129 loop homeostasis. Moreover, R-loop regions impacted by cellular A3B show significant
130 enrichments for APOBEC3 signature mutations including *kataegis* in breast tumors.
131 Altogether, these results reveal an unanticipated role for A3B in R-loop biology and a
132 distinct mechanism of transcription-associated cancer mutagenesis.

133

134 **Results**

135

136 **APOBEC3B interacts with R-loops and R-loop-associated proteins**

137 Little is known about the molecular processes that serve to regulate the mutagenic
138 activities of A3B. To address this gap in knowledge, a functional A3B-2xStrep-3xFlag
139 construct (hereafter A3B-SF) was expressed in 293T cells, anti-Strep affinity-purified,
140 and subjected to mass spectrometry to identify interacting proteins (AP-MS workflow
141 schematic in **Fig. S1a**). This procedure included exogenous RNase A and high salt
142 concentrations to enrich for direct and strong interactions, respectively. Immunoblots,
143 Coomassie gels, and DNA deaminase activity assays were used to validate the
144 presence, enrichment, and activity of affinity-purified A3B (**Fig. S1b-d**). Expression of
145 an eGFP-SF construct and an empty 2xStrep-3xFlag vector was analyzed in parallel as
146 negative controls.

147 Six independent AP-MS experiments yielded a total of 24 specific A3B-
148 interacting proteins (**Table S1**; independent confirmation in **Fig. S1e-f**). These proteins
149 were abundant in all 6 A3B-SF data sets and, importantly, absent in GFP-SF or empty
150 vector datasets. Only CDK4, which regulates A3B localization during the cell cycle⁵⁴,
151 and hnRNPUL1, which tethered to Cas9 is capable of targeting A3B for base editing⁵⁵,

152 had been reported previously. However, literature analyses revealed that 60% of these
153 A3B interactors had been found independently in S9.6 AP-MS experiments⁵³ (**Fig. 1a-**
154 **b**). As the S9.6 mAb binds strongly to RNA/DNA hybrid structures^{56,57}, this significant
155 interactome overlap suggested that A3B may also interact with R-loops. To test this
156 hypothesis, interactions between A3B and multiple R-loop factors were confirmed in co-
157 immunoprecipitation (co-IP) experiments. For example, doxycycline (Dox)-inducible
158 A3B-eGFP was immunoprecipitated from MCF10A cells with an anti-eGFP antibody and
159 the R-loop-associated protein hnRNPUL1 was detected by immunoblotting (system
160 validation in **Fig. 1c** and representative co-IP in **Fig. 1d**). Parallel slot blots showed that
161 R-loops also co-purified with A3B-eGFP, and the RNase H sensitivity of the signal
162 demonstrated the specific detection of RNA/DNA hybrids (**Fig. 1d**).

163 The S9.6 mAb was then used to IP RNA/DNA hybrids from MCF10A cells treated
164 with phorbol 12-myristate 13-acetate (PMA) to induce endogenous *A3B* expression⁵⁸.
165 Immunoblotting confirmed enrichment of an established R-loop interacting protein,
166 TOP1^{59,60}, and a shared R-loop and A3B interactor, hnRNPUL1, in all S9.6 IP reactions
167 except those saturated with a synthetic RNA/DNA hybrid competitor (**Fig. 1e**). The non-
168 R-loop-interacting protein Lamin B1 served as a negative control for these IP reactions.
169 Endogenous A3B copurified with R-loop structures in basal non-induced conditions and
170 this interaction increased following PMA treatment (**Fig. 1e**). Importantly, no A3B signal
171 was detected in S9.6 pull downs from *A3B*-null MCF10A cells, which demonstrated
172 interaction specificity (**Fig. 1e**; *A3B* knockout construction and validation in **Fig. S2a-d**).

173

174 **Elevated nuclear R-loop levels in *A3B*-null and *A3B*-depleted cells**

175 To investigate a potential role for A3B in R-loop biology, R-loop levels were quantified in
176 MCF10A and its *A3B*-null derivative. First, nucleoplasmic S9.6 staining intensity was
177 measured by immunofluorescence (IF) confocal microscopy. These experiments
178 revealed a strong increase in nucleoplasmic S9.6 fluorescence in *A3B*-null cells in
179 comparison to parental MCF10A cells (**Fig. 2a-b**). Second, S9.6 dot blot experiments
180 confirmed elevated R-loop levels in the *A3B*-null MCF10A cells in comparison to the
181 parental line (**Fig. 2c-d**). Importantly, in both series of experiments, RNase H treatment
182 eliminated the increase in R-loop signals observed in the absence of endogenous A3B.
183 S9.6 signal detecting nucleolar rRNA is mostly insensitive to RNase H treatment, as
184 reported⁶¹, and is also largely unaffected by A3B.

185 To address whether the relationship between A3B and R-loop levels may be a
186 general mechanism, analogous S9.6 IF microscopy and dot blot experiments were done
187 using U2OS cells, which express high levels of endogenous A3B^{54,62,63}. U2OS cells
188 were transduced with a validated shRNA to stably deplete endogenous *A3B* or a non-
189 targeting control shRNA^{22,64} (*A3B* knockdown validation in **Fig. S2e-g**). In these
190 experiments, *A3B* knockdown caused a strong increase in nucleoplasmic S9.6 staining
191 intensity by IF microscopy in comparison to control transduced cells analyzed in parallel
192 (**Fig. 2e-f**). As above, nearly all nucleoplasmic S9.6 staining was ablated by RNase H
193 treatment, indicating that the signal is specific to RNA/DNA hybrids. An increase in
194 RNA/DNA hybrid signal was also obtained in S9.6 dot blot experiments from *A3B*-
195 depleted versus control transduced cells and, again, specificity was confirmed by
196 RNase H treatment (**Fig. 2g-h**). R-loop imbalances are a known source of DNA
197 damage³⁸⁻⁴⁰, and elevated R-loop levels in *A3B*-null MCF10A and *A3B*-depleted U2OS

198 cells triggered concomitant increases in DNA break formation as evidenced by γ -H2AX
199 staining (**Fig. 2i-l**). However, it is important to note that these elevated levels of R-loops
200 and DNA damage did not alter overall rates of DNA replication (EdU incorporation) or
201 cell cycle progression (**Fig. S2h-k**).

202

203 **A3B reduces nuclear R-loop levels through a deamination-dependent mechanism**

204 Given results above showing increased R-loop accumulation upon *A3B* loss, we next
205 asked whether A3B overexpression might have the opposite effect and suppress R-loop
206 formation. U2OS cells were transfected with an expression vector for A3B-eGFP or
207 eGFP as a negative control, incubated 24 hrs to allow for protein expression, treated 4
208 hrs with the Bromodomain and Extra-Terminal (BET) protein family inhibitor JQ1 to
209 enhance R-loop formation^{44,65,66}, and then analyzed by IF confocal microscopy for S9.6
210 staining. In comparison to the eGFP control, A3B-eGFP expression caused a significant
211 decrease in the average intensity of nucleoplasmic S9.6 levels (**Fig. 3a-b**). Interestingly,
212 expression of A3A, which is more active than A3B in ssDNA deamination assays^{67,68},
213 had no effect suggesting a specific R-loop role for A3B (**Fig. 3a-b**).

214 The hallmark biochemical activity of A3B is ssDNA C-to-U deamination (e.g.,
215 refs.^{22,67,68}; reviewed by refs.^{13,69,70}). To determine whether deaminase activity is
216 required for reducing nuclear R-loop levels, U2OS cells were transfected with constructs
217 expressing A3B-eGFP or a single amino acid substitution catalytic mutant E255A, which
218 prevents A3B from deprotonating water and creating the hydroxide ion required for C-to-
219 U deamination (reviewed by refs.^{13,69,70}). Importantly, wild-type A3B caused a significant
220 reduction in nucleoplasmic R-loop levels as quantified by S9.6 staining and IF

221 microscopy, whereas the catalytic mutant had a less pronounced effect despite similar
222 expression levels (**Fig. 3c-d** and data not shown). However, because U2OS cells
223 already express high levels of endogenous A3B (above) and APOBEC3 enzymes
224 including A3B are reported to oligomerize^{68,71-75}, this intermediate phenotype may be
225 due to oligomerization between overexpressed mutant and endogenous A3B.

226 Therefore, a series of genetic complementation experiments was performed to
227 compare the activities of wild-type A3B and the E255A catalytic mutant in cells lacking
228 endogenous A3B. First, endogenous *A3B* was depleted from U2OS cells as above,
229 which resulted in lower A3B protein and activity levels (**Fig. 3e**). Second, *A3B*-depleted
230 U2OS cells were stably transfected with shRNA-resistant constructs expressing HA-
231 tagged wild-type A3B, A3B-E255A, or an empty vector control (**Fig. 3e**). The wild-type
232 A3B enzyme but not the E255A catalytic mutant restored ssDNA deaminase activity as
233 expected (**Fig. 3e**). Third, R-loop levels were analyzed by S9.6 dot blot assays.
234 Importantly, complementation with wild-type A3B rescued the effect of *A3B* depletion
235 and caused a significant reduction in R-loops (**Fig. 3f-g**). In contrast, cells
236 complemented with similar levels of the catalytic mutant protein, A3B-E255A, showed
237 no significant change in R-loop levels demonstrating a deamination-dependent
238 mechanism.

239

240 **APOBEC3B-regulated R-loops are transcription-dependent**

241 R-loop formation normally occurs during the process of transcription when a nascent
242 RNA hybridizes with the template DNA strand and displaces the non-template ssDNA
243 behind the elongating RNA polymerase (reviewed by refs.^{38,39,76}). To confirm that A3B-

244 associated R-loops are transcription-dependent, shCtrl and shA3B U2OS cells were
245 treated with the global transcription inhibitor triptolide^{77,78} and IF microscopy analyses
246 were used to quantify R-loop levels. As above, A3B depletion resulted in an increase in
247 nucleoplasmic R-loop levels, and triptolide abolished this effect (**Fig. 4a-b**). Dot blot
248 analysis of RNA/DNA hybrids yielded similar results (**Fig. 4c-d**). Complementary data
249 were obtained using a different transcription inhibitor, flavopiridol, which specifically
250 inhibits the CDK9 kinase subunit of the positive transcription elongation factor b (P-
251 TEFb) of RNA polymerase II (*i.e.*, flavopiridol inhibits CDK9, blocks transcription
252 elongation, and concomitantly blocks R-loop accumulation⁷⁹) (**Fig. 4c-d**). These results
253 confirmed that A3B-targeted R-loops are indeed transcription-dependent.

254

255 **APOBEC3B alters the genome-wide distribution of R-loops**

256 The aforementioned IF confocal microscopy and dot blot results suggested a role for
257 A3B in regulating R-loop levels genome-wide. This possibility was investigated using
258 DNA/RNA hybrid IP (DRIP)-seq experiments. In line with previous studies⁷⁹⁻⁸¹, DRIP-
259 seq peaks in wild-type (WT) and A3B knockout (KO) MCF10A cells were mainly
260 intragenic and distributed between protein-coding, long non-coding RNA, and enhancer
261 RNA genes (**Fig. 5a-b**). As anticipated by these distributions and the transcription
262 dependence above, the vast majority of DRIP-seq positive regions in WT and KO
263 MCF10A cells occurred in expressed genes (**Fig. S3a**).

264 A global comparison of DRIP-seq peaks between KO and WT MCF10A revealed
265 changes in the overall R-loop landscape with 8,296 peaks 'increased', 13,761 peaks
266 'decreased', and 154,036 peaks 'unchanged' (red vs blue traces in **Fig. 5c-e**).

267 Representative individual gene results are shown for *GADD45A* and *PHLDA1*,
268 *HIST1H1B* and *SYT8*, and *HIST1H1E* and *DDX1*, which show increased, decreased,
269 and unchanged R-loop levels, respectively, in KO cells in comparison to WT cells (**Fig.**
270 **5f, h, j**). These DRIP-seq results were confirmed by gene-specific DRIP-qPCR (**Fig. 5g,**
271 **i, k**). As above, DRIP-qPCR signals were reduced significantly by RNase H treatment,
272 further confirming R-loop specificity (**Fig. 5g, i, k, striped bars**). Differential DRIP signals
273 were not due to transcription differences between the KO and WT cell lines (**Fig. S3b**).
274 As expected, negligible DRIP signals were found in non-expressed genes and
275 intergenic loci (e.g., *TFF1* in **Fig. S3c-d**). In addition, similar DRIP results were obtained
276 in a different cell line (*A3B*-depleted HeLa) analyzed by immunoblotting and qPCR (**Fig.**
277 **S3e-g**).

278

279 **APOBEC3B accelerates the kinetics of R-loop resolution**

280 Transcriptional activation by different signal transduction pathways is known to trigger
281 large increases in R-loop formation^{82,83}. As the datasets above were generated under
282 normal growth conditions, an additional set of experiments was done to address
283 whether *A3B* may also affect signal transduction-induced R-loops. Therefore, WT and
284 KO MCF10A lines were treated with PMA to induce the protein kinase C (PKC) and
285 non-canonical (nc)NF- κ B signal transduction pathways and, as such, activate the
286 transcription of many genes including endogenous *A3B*^{58,84}.

287 First, global R-loop distributions were analyzed by DRIP-seq in WT MCF10A
288 following 2 hrs PMA treatment in comparison to a DMSO control treatment (workflow in
289 **Fig. S4a**). As anticipated, PMA caused changes in the overall R-loop landscape with

290 13,422 peaks increased, 16,432 peaks decreased, and 171,322 unchanged (**Fig. S4b-**
291 **d**). Many genes such as *JUNB* and *FOS* were induced strongly by PMA treatment and
292 showed significant increases in DRIP signals (**Fig. S4e-f**). Other genes such as *NAXE*
293 and *ARL4D* showed decreases in DRIP signals (**Fig. S4g-h**), whereas the majority such
294 as *GAPDH* and *GEMIN7* showed no changes in R-loop formation (**Fig. S4i-j**).

295 Second, a parallel set of ChIP-seq experiments was done in MCF10A with Dox-
296 inducible A3B-eGFP (**Fig. 1c**) to assess whether any of these R-loop categories might
297 be bound by this deaminase (workflow in **Fig. S4a**). An epitope-tagged protein was
298 necessary because ChIP-grade antibodies have yet to be developed for endogenous
299 A3B. Interestingly, A3B-eGFP appeared to bind preferentially to genomic DNA regions
300 coincident with DRIP-seq peaks increased in PMA-treated cells in comparison to vehicle
301 control treated cells (ChIP-seq results superimposed over DRIP-seq results in **Fig.**
302 **S4b**). In contrast, A3B-eGFP ChIP-seq peaks were mainly unperturbed in genomic DNA
303 regions in which R-loop levels decreased or remained unchanged upon PMA treatment
304 (**Fig. S4c-d**). Representative results were confirmed independently by ChIP-qPCR (**Fig.**
305 **S4k**). Moreover, quantification indicated that 43% of A3B ChIP peaks overlap with R-
306 loops peaks induced by PMA ($P = 0.0001$, two-tailed binomial test; 54% overlap for
307 ChIP peaks with >5-fold enrichment compared to uninduced Dox⁻ condition, $P =$
308 0.0008). These results combined to indicate that A3B binds preferentially to genomic
309 DNA regions with evidence for R-loop accumulation.

310 Third, the PMA-inducibility of this system enabled an assessment of the kinetics
311 of R-loop resolution in the presence and absence of A3B. WT and KO cells were treated
312 with PMA or DMSO for 2 and 6 hrs and then analyzed by DRIP-seq (workflow in **Fig.**

313 **6a**). These timepoints were chosen for analysis because transcription induction and R-
314 loop formation are rapid (2 hrs data above) and A3B protein levels are upregulated
315 maximally by 6 hrs post-PMA treatment⁵⁸ (**Fig. 6b-c**). For example, *JUNB* and *DUSP1*
316 have R-loop peaks that are strongly induced by PMA at 2 hrs and these return to near-
317 control levels by 6 hrs (**Fig. 6d**). In contrast, R-loop peaks in the same genes remained
318 significantly elevated and/or showed delayed resolution kinetics in KO cells after 6 hrs
319 PMA treatment (**Fig. 6d**). PMA non-responsive genes used as controls did not show R-
320 loop induction or major differences in R-loop levels after 6 hrs PMA treatment (e.g.,
321 *GAPDH* and *HSPA8* in **Fig. 6e**). Moreover, independent IF confocal microscopy studies
322 of the kinetics of R-loop resolution following PMA treatment of WT MCF10A cells
323 showed that nucleoplasmic R-loop levels peak at 2 hrs and decline substantially by 6
324 hrs, whereas no decline (even a modest increase) was observed in A3B KO cells (**Fig.**
325 **6f-g**). As above, all DRIP-qPCR and nucleoplasmic R-loop signals were sensitive to
326 RNase H treatment indicating specificity (**Fig. 6d-g**). Taken together with the ChIP data
327 above, the results of these PMA time course experiments indicated that nuclear A3B is
328 recruited to PMA-induced R-loops and contributes to their timely resolution.

329

330 **APOBEC3B biochemical activities required for R-loop resolution**

331 To investigate the biochemical activities of A3B in R-loop resolution, wild-type A3B was
332 purified from 293T cells (**Fig. S5a**) and used for nucleic acid binding and DNA
333 deamination experiments (**Fig. 7** and **Fig. S5b-c**). The various nucleic acids used in
334 these biochemical experiments are depicted in **Fig. 7a**. EMSAs indicated that A3B is
335 capable of binding to R-loop structures (novel), to ssDNA and ssRNA (expected^{67,68,85}),

336 and to lesser extents to dsDNA, dsRNA, or RNA/DNA hybrid (also expected^{67,68,85}; **Fig.**
337 **S5b-c**). These native EMSAs were hard to quantify due to accumulation of large
338 protein/nucleic acid complexes in the wells. We therefore reduced the complexity of
339 binding studies by quantifying the release of fluorescently-labeled ssRNA and ssDNA
340 from A3B by incubating with a broad concentration range of otherwise identical
341 unlabeled nucleic acid competitors. These experiments demonstrated that A3B binds
342 strongly and nearly indistinguishably to both ssRNA and ssDNA (**Fig. 7b**).

343 RNA is an inferred inhibitor of the ssDNA cytosine deaminase activity of A3B
344 based on experiments in which exogenous RNase A treatment is required to detect
345 ssDNA deaminase activity in cancer cell extracts (e.g., refs.^{22,58}). We therefore
346 wondered whether the RNA in R-loop structures might inhibit the ssDNA deaminase
347 activity of A3B on the unpaired ssDNA strand. Qualitative single timepoint reactions
348 indicated clear activity on free ssDNA cytosines and potentially reduced activities on
349 ssDNA cytosines in a bubble, short R-loop, and long R-loop structures (**Fig. 7c**). A
350 quantitative time course comparing A3B activity on free ssDNA versus ssDNA in the
351 context of an R-loop structure indicated that the latter substrate is only about 2-fold less
352 preferred (**Fig. 7d**). These data showed that R-loops can be substrates for A3B-
353 catalyzed ssDNA deamination. The 2-fold diminution in activity may be due to ssDNA
354 inaccessibility caused by the relatively short nature of the synthetic R-loop (21
355 nucleotides) and/or to competition with unpaired ssDNA or ssRNA.

356 To gain additional mechanistic insights into A3B function in R-loop biology, we
357 analyzed the nucleoplasmic R-loop phenotypes of an A3B mutant defective in nuclear
358 localization (Mut1)⁸⁶ and a mutant incapable of binding strongly to nucleic acid (Mut2)⁸⁵.

359 Both of these activities are governed by the N-terminal domain (NTD) of A3B, and are
360 independent of the C-terminal domain (CTD) that binds much more weakly to ssDNA
361 and catalyzes deamination^{67,85,86}. We confirmed the nuclear localization defect of the
362 Mut1 and, interestingly, showed that Mut2 still retains this hallmark activity (**Fig. 7e**).
363 Mut2 was also purified and, in contrast to the wild-type enzyme, confirmed defective in
364 binding to ssRNA and ssDNA using EMSAs (**Fig. S5a** and **Fig. 7f**). However, Mut2 still
365 retained high levels of ssDNA deaminase activity and was similarly active on free
366 ssDNA and short R-loop ssDNA (**Fig. 7g**). This result is consistent with the possibility
367 that unannealed nucleic acid may interfere with the deaminase activity of the WT
368 enzyme (above) but not with Mut2, which has reduced nucleic acid binding activity.
369 Most importantly, in contrast to WT A3B, neither mutant was capable of decreasing
370 nucleoplasmic R-loop levels following JQ1 treatment (**Fig. 7h**). The separation-of-
371 function Mut2 protein also had a diminished capacity to co-IP interactors (**Fig. S1f**).
372 These results indicated that both nuclear localization and nucleic acid binding activities
373 are required for A3B to alter nucleoplasmic R-loop levels.

374

375 **Genome-wide associations between APOBEC3 signature mutations, gene** 376 **overexpression, and splicing defects**

377 The involvement of A3B in transcription-dependent R-loop biology led us next to
378 evaluate whether transcribed genes may be preferred sites of mutagenesis. Specifically,
379 we propose a working model in which exposed ssDNA cytosines in R-loop regions are
380 deaminated by A3B and resolved into mutagenic or non-mutagenic outcomes (**Fig. 8a**
381 and **Discussion**). Non-mutagenic outcomes are likely to comprise most resolution

382 events, but these leave no genomic scars and, thus, are invisible to bioinformatics
383 analyses. However, mutagenic R-loop resolution outcomes are predicted to reflect the
384 intrinsic structural preference of A3B for deamination of cytosines in TC motifs^{7,87,88} and
385 more broadly in TCW and RTCW extended motifs as defined experimentally and
386 computationally^{23,26}. For comparison, A3A elicits a preference for YTCW^{23,26,89}.

387 One prediction of this model is that a positive association may exist between
388 transcription levels and APOBEC3-attributed mutations. Because previous studies
389 established a correlation between gene expression and R-loop formation⁷⁹, we
390 predicted that higher rates of transcription should, at least at some loci, lead to higher
391 rates of R-loop formation and increased exposure to A3B. This idea was addressed
392 using whole-exome sequenced (WES) breast cancers and corresponding RNA-seq data
393 from TCGA project as well as whole-genome sequenced (WGS) breast cancers from
394 the ICGC consortium and normal breast tissue gene expression data from the GTEx
395 project (Methods). An initial association between gene expression levels and
396 APOBEC3-attributed mutations was intriguing but became insignificant after accounting
397 for gene size (**Fig. S6a-b**). However, a strong positive association emerged between
398 the magnitude of gene overexpression in breast cancer compared to normal breast
399 tissue and the proportion of mutations attributable to APOBEC3 deamination (all TCW
400 mutations in **Fig. 8b**, $P < 1.0 \times 10^{-12}$ by student's t-test; RTCW/YTCW breakdown in **Fig.**
401 **S6c**). These analyses indicated that the higher the degree of gene overexpression in
402 breast cancer the higher the proportion of mutations attributable to APOBEC3, with the
403 highest overexpressed gene group showing an average of over 50-fold more APOBEC3
404 signature mutations than any of the three lowest expressed gene groups.

405 Second, because splicing defects lead to increases in R-loop formation⁹⁰⁻⁹², our
406 working model predicts that splice factor mutant tumors may manifest elevated levels of
407 APOBEC3 signature mutations. This idea was investigated by splitting the TCGA breast
408 cancer WES data set into tumors with and without mutations in splice factor genes and
409 evaluating associations with the proportion of mutations attributable to APOBEC3
410 activity. Remarkably, 53% of the breast tumors with mutant splice factor genes (43/81)
411 had significant levels of APOBEC3 signature mutations (**Fig. 8c**). In contrast, only 35%
412 of breast tumors without mutations in the same splice factor gene set (326/841) showed
413 a detectable APOBEC3 mutation signature (**Fig. 8c**; $P < 0.017$ by Fisher's exact test).
414 APOBEC3-attributed mutations in both groups were partitioned into RTCW/YTCW
415 tetranucleotide motifs and, interestingly, the A3B-associated RTCW motif was only
416 absent from one of the splice factor mutant tumors (1/43) in comparison to a significant
417 proportion of the non-splice factor mutant group (52/326) (**Fig. S6d-e**; $P = 0.028$ by
418 Fisher's exact test). Splice factor mutant tumors also had a higher mean percentage of
419 APOBEC3-attributed mutations (39% vs 31%, respectively; $P = 0.042$ by unpaired two-
420 sample Welch's t-test) as well as higher total numbers of mutations on average than
421 non-splice factor mutated samples ($P = 0.0018$ by Welch's two sample t-test). Even the
422 top quartile of tumors with the strongest APOBEC3 signature had higher total numbers
423 of mutations in the splice factor mutant group ($P = 0.0095$ by Welch's two sample t-test).
424 These relationships between splice factor defects, higher mutation loads, and
425 APOBEC3 mutation signature are not likely due to chance because no other similarly
426 sized gene set selected randomly from housekeeping genes (100,000 random gene set
427 selections) is similarly mutated in TCGA breast cancer data sets (*i.e.*, the observed

428 splice factor defects are not due to higher rates of mutation; rather, the observed splice
429 factor defects are likely to contribute to the higher rates of mutation). We also noted that
430 APOBEC3-attributed mutations accumulate preferentially on the non-transcribed strand
431 (NTS) over the transcribed strand (TS) in both splice factor mutant and non-mutant
432 tumor groups with a statistical difference that may relate to the underlying mechanism
433 ($P = 0.0284$ and $P = 4.3 \times 10^{-12}$, respectively, by student's t-test). In further support of a
434 connection between aberrant splicing, R-loop formation, and APOBEC3 mutagenesis,
435 A3B overexpression suppresses the increase in R-loop formation caused by treating
436 U2OS cells with the splicing inhibitor pladienolide B (Plad B; **Fig. 8d**).

437 Third, because APOBEC3 signature *kataegic* events are undoubtedly due to
438 strand-coordinated deamination by at least one APOBEC3 enzyme^{20,25}, we asked what
439 proportion of these events occur in genes and, moreover, occur on the NTS versus the
440 TS to potentially reveal which part of the genome may be more susceptible. This
441 analysis focused again on breast cancer due to the large size and overall high quality of
442 the WGS data sets. A global mapping of all *kataegis* events in primary breast
443 adenocarcinomas from the Pan-Cancer Analysis of Whole Genomes (PCAWG)
444 revealed a bimodal distribution with one peak located within 1 kbp of a structural
445 variation breakpoint (SV) and another similarly sized peak much further away from the
446 nearest SV (~1 Mbp; $n = 198$ WGS data sets; blue bars in **Fig. 8e**). As expected⁹³, the
447 SV-proximal subset of *kataegis* events is likely due to deamination of resected ssDNA
448 ends during recombination repair. Also expected, non-clustered (*i.e.*, dispersed)
449 APOBEC3-attributed mutations occur on average of >1 Mbp apart (yellow bars in **Fig.**
450 **8e**). In contrast, the majority of APOBEC3-attributed *kataegic* events (>75%) map >10

451 kbp away from SVs and are unlikely to be due to a DNA double-stranded break and
452 recombination-associated mechanism (red bars in **Fig. 8e**). Moreover, a significant
453 proportion of these distal APOBEC3 signature *kataegic* events occur within R-loop
454 regions defined above in DRIP-seq experiments.

455 To investigate the source of APOBEC3 signature *kataegis*, we plotted overall
456 enrichments for A3B-associated RTCA and A3A-associated YTCA tetranucleotide
457 motifs (R=A or G; Y=C or T)²⁶ and shaded data points red to distinguish breast tumors
458 with at least one R-loop associated *kataegic* event. This analysis indicated, first, that
459 tumors with APOBEC3 signature *kataegis* are common and, second, that APOBEC3
460 *kataegic* mutations overlapping R-loop regions, in contrast to dispersed APOBEC3
461 mutations, are skewed toward RTCA motifs (**Fig. 8f-g**; Q-values in each dot plot
462 determined using Mann-Whitney U-tests). Third, the overall RTCW skew of *kataegic* (≥ 3
463 mutations per cluster) versus dispersed APOBEC3 mutations was greatest for
464 mutations occurring on the NTS but still evident on the TS and intergenic regions (**Fig.**
465 **8f**; $P = 0.0006$, $P = 0.0086$, and $P = 0.096$ respectively, by Fisher's exact tests after
466 FDR correction). For greater stringency, this latter analysis was repeated for longer
467 APOBEC3 *kataegic* tracts (≥ 5 mutations per cluster) and a statistically significant
468 enrichment was only evident for RTCA events on the NTS of genes [**Fig. 8g**; $P = 0.0001$
469 (NTS), $P = 0.15$ (TS), and $P = 0.072$ (intergenic)]. Representative NTS *kataegic* events
470 are shown for *PRKCA* and *LGR5* (**Fig. 8h**). Taken together, these different bioinformatic
471 analyses support a model in which at least a subset of R-loop structures is susceptible
472 to C-to-U deamination events most likely catalyzed by A3B.

473

474 **Discussion**

475 Our studies are the first to report the cellular interactome of A3B and reveal an
476 unanticipated role for this antiviral enzyme in R-loop biology. We delineate a functional
477 relationship between A3B and R-loops with higher R-loop levels occurring upon A3B
478 knockout/down and lower R-loop levels upon A3B overexpression. Genome-wide DRIP-
479 seq experiments in physiological conditions and upon activation of a signal transduction
480 pathway indicated that thousands of R-loops in cells are affected by A3B (*i.e.*, increased
481 or decreased in *A3B*-null cells). This number represents over 10% of R-loops genome-
482 wide, which is comparable to the proportions of R-loops affected by other R-loop
483 regulatory factors, such as TOP1, DDX5, XRN2, and PRMT5^{80,94}. These findings are
484 also in line with knowledge that multiple proteins contribute to R-loop regulation,
485 including RNase H1, TOP1, SETX, AQR, UAP56/DDX39B, FANCD2, and
486 BRCA1/2^{38,45,80,94-103}. Determining the precise combination of molecular mechanisms
487 responsible for the regulation of a given R-loop remains a challenge for future studies.

488 In addition to discovering an unanticipated role for A3B in R-loop homeostasis,
489 our studies also shed light on the underlying molecular mechanism of R-loop resolution.
490 First, complementation experiments showed that the mechanism is deaminase-
491 dependent with expression of a single amino acid catalytic mutant (E255A) failing to
492 decrease nucleoplasmic R-loop levels. Second, the nuclear localization activity of A3B
493 is essential. This requirement may seem obvious but is important to help rule-out
494 potential indirect effects such as A3B binding to cytoplasmic factors and affecting their
495 import into the nuclear compartment and participation in R-loop formation. Third, A3B is
496 capable of binding to R-loop structures, and the strong nucleic acid binding activity of

497 A3B is required for suppressing nucleoplasmic R-loop levels. Our biochemical
498 competition experiments indicated that ssRNA and ssDNA binding activities are
499 comparable in strength. Together with the fact that A3B's strong nucleic acid binding
500 activity resides within the N-terminal half of the protein and the weaker ssDNA binding
501 activity required for catalysis is governed by the C-terminal half of the enzyme, we favor
502 a working model in which direct binding of A3B to nascent ssRNA adjacent to R-loops
503 and/or to ssDNA exposed in R-loop structures is critical for R-loop regulation (**Fig. 8a**).
504 The next steps in such a mechanism may be deamination of exposed ssDNA cytosines
505 in R-loop structures, uracil excision by UNG2, ssDNA breakage by APEX, and
506 recruitment of additional downstream repair factors for resolution, by analogy to the
507 resolution of AID-catalyzed R-loop associated deamination events in immunoglobulin
508 gene switch regions^{41,42} and APOBEC-catalyzed editing of R-loop DNA cytosines
509 exposed in Cas9-mediated base editing reactions¹⁰⁴. Additional tests of this model
510 should consider complications from synthetic lethal interactions such as between A3B
511 overexpression and UNG2 inhibition⁵². Moreover, the relationship between R-loop
512 homeostasis and DNA repair is likely to be complex, and it is easy to imagine how
513 perturbing R-loop levels in either direction (up or down) could lead to elevated DNA
514 damage responses (e.g., γ -H2AX accumulation), as observed here with A3B-deficient
515 cells and elsewhere with other factors^{80,95,96,99,105,106}. Notably, forced overexpression of
516 A3B can also cause elevated DNA damage responses including γ -H2AX
517 accumulation^{22,52,107}.

518 This proposed mechanism is likely to lead to predominately error-free resolution,
519 which cannot be detected by bioinformatic genomic analyses. However, a subset of the

520 uracil lesions and/or abasic sites may lead to APOBEC3 signature mutations and, if
521 clustered, to APOBEC3 *kataegic* events. The possibility of such mutagenic outcomes is
522 supported by a dose-responsive association between genes overexpressed in breast
523 cancers compared to normal breast tissue and the proportions of somatic mutations
524 attributed to APOBEC3 deamination (**Fig. 8b**). Moreover, a preferential accumulation of
525 APOBEC3-attributed mutations is also observed in splice factor mutant breast tumors
526 (**Fig. 8c**). As transcription and splicing are interconnected processes¹⁰⁸ and splice factor
527 defects are known to increase R-loop levels^{90-92,109}, it is easy to imagine how
528 perturbations in these processes may contribute to increased R-loop formation and
529 exposures of single-stranded cytosines to APOBEC3 deaminase activity. This possibility
530 is further supported by recent bioinformatic studies indicating higher APOBEC3
531 mutation densities on the NTS of actively expressed genes (including the
532 overexpressed genes analyzed here) in multiple cancer types¹¹⁰. We cannot exclude
533 the possibility that other APOBEC3 enzymes, most notably A3A, may also be able to
534 contribute to R-loop mutation. However, this alternative is disfavored because A3A
535 overexpression does not affect R-loop levels and, importantly, the majority of APOBEC3
536 *kataegic* events are observed far away from sites of structural variation and are
537 enriched for mutations in A3B-associated 5'-RTCW motifs (**Fig. 8e-h**).

538 In addition, because a proportion of APOBEC3 mutagenesis is likely due to
539 deamination of lagging-strand templates during DNA replication^{29-31,33,34,94}, it is
540 important to emphasize that APOBEC3-catalyzed C-to-U lesions in transcription-
541 associated R-loop structures are likely to attract different subsets of DNA repair
542 enzymes. A uracil in the DNA replication template strand will instruct the proper

543 insertion of an adenine in the nascent strand, which leaves a U:A base pair for UNG2
544 recognition and faithful uracil base excision repair with the net result being a C-to-T
545 transition. A uracil in an R-loop, following R-loop resolution, will lead to a U/G mispair,
546 which may similarly template the insertion of an adenine through replication but can also
547 attract mismatch repair enzymes, which could promote the creation of a longer ssDNA
548 tract and additional APOBEC3 mutagenesis. This possibility is supported by recent
549 results showing a mismatch repair-dependent synthetic lethal interaction between A3B
550 activity and uracil excision repair disruption⁵² and a role for mismatch repair in the
551 creation of *omikli* (shorter-than-*kataegic* tracts of APOBEC3-attributed mutations)¹¹¹. It
552 is also supported by precedents with AID-dependent antibody gene diversification in B
553 lymphocytes where both uracil base excision repair and mismatch repair have integral
554 roles^{41,42}. Of course, uracil lesions in both DNA replication template strands and R-loops
555 can lead to alternative outcomes including uracil excision, abasic site bypass or
556 cleavage, single- and double-stranded DNA breaks, and larger-scale genetic
557 aberrations including translocations. A3B-mediated mutagenesis may be particularly
558 relevant in cancer cells that display both increased A3B expression and R-loop
559 dysregulation resulting from mutations in splice factors or other R-loop regulatory
560 factors (e.g., BRCA1/2 and Fanconi anemia proteins^{99,100,102,112,113}) and/or activation of
561 signal transduction pathway-induced transcriptional programs^{82,83} such as during
562 conditions of oncogenic signaling, infection, or inflammation^{58,114,115}. Therefore, in
563 addition to archetypic base substitution mutations, it is tempting to speculate that at
564 least some R-loop-associated DNA damage and chromosome aberrations (reviewed by
565 refs.^{39,46,48,116}) may be instigated by the A3B-dependent mechanism described here.

566 In addition to the resolution mechanism discussed above, a potentially
567 overlapping alternative is A3B-dependent recruitment of other proteins known to
568 promote R-loop resolution. Such interactions could be direct or bridged, for instance, by
569 RNA or ssDNA. In support of this possibility, the A3B separation-of-function mutant
570 Mut2, which is deficient in nucleic acid binding but proficient in nuclear import and DNA
571 deamination, is less capable of interacting with several R-loop associated factors (Fig.
572 S1f). Moreover, although our studies here focused on AP-MS interactions specific to
573 A3B (absent from all controls), a number of A3B-enriched factors (present at lower
574 levels in at least one control reaction), such as the helicase DHX9, might be worthy of
575 future investigation. This DNA/RNA helicase was reported recently as a suppressor of
576 the antiviral activity of A3B¹¹⁷. It is harder to envisage a mechanism to explain the
577 subset of genes that elicit decreased R-loop levels in the absence of A3B. In these
578 instances, A3B may be blocking a known resolution activity, such as a helicase that
579 loads via RNA or ssDNA, from gaining access to R-loops. Further studies on A3B
580 regulation of R-loop homeostasis will undoubtedly be exciting as answers will shed
581 additional light on R-loop biology, provide insights into the normal physiological
582 functions of A3B in innate antiviral immune responses, and may help define additional
583 targetable nodes in A3B-overexpressing tumor types such as breast cancer.

584

585 **Acknowledgements**

586 We thank N.J. Proudfoot for critically reading the manuscript, J. Becker and J. Duda for
587 corroborative localization data with A3B mutants, the University of Minnesota Imaging
588 Center for access to instrumentation, and the Oxford Genomics Centre at the Wellcome

589 Centre for Human Genetics (funded by Wellcome Trust grant 203141/Z/16/Z) for the
590 generation and initial processing of the sequencing data. This work was supported by
591 NCI P01 CA234228 (to RSH), NIAID R37 AI064046 (to RSH), and by the University of
592 Minnesota Masonic Cancer Center, Academic Health Center, and College of Biological
593 Sciences. NG lab is supported by the Royal Society University Research fellowship
594 (BVD07340), Royal Society Enhancement Award (RGF\EA\180023) and EPA Research
595 Fund (Sir William Dunn School of Pathology, University of Oxford) to NG and CRUK
596 development fund (CRUK DF-0119) to AC and NG. MT and SM are supported by the
597 Wellcome Trust Investigator Award to SM (WT210641/Z/18/Z). KMM lab was supported
598 by NCI RO1 CA198279 and NCI RO1 CA201268. LBA lab was supported by US NIH
599 R01 ES030993 and R01 ES032547. Salary support for JLM was provided initially by an
600 NSF Graduate Research Fellowship (Grant Number 00039202) and subsequently by
601 HHMI. Salary support for MCJ was provided in part by T32 CA009138 and
602 subsequently NCI F31 CA243306. Salary support for BS was provided by HHMI with
603 some supplies provided by the Ovarian Cancer Research Alliance (Ann and Sol
604 Schreiber Mentored Investigator Award 812337). Salary support for DJS was provided
605 by NIAID K99 AI147811. RSH is the Margaret Harvey Schering Land Grant Chair for
606 Cancer Research, a Distinguished University McKnight Professor, and an Investigator
607 of the Howard Hughes Medical Institute.

608

609 **Author contributions**

610 R.S.H., J.L.M., A.C. and N.G. conceived and designed these studies. J.L.M. and A.C.
611 performed experiments unless otherwise noted. E.K.L. generated U2OS knockdown

612 and complement cell lines along with assisted in tissue culture and genomic DNA
613 isolations for dot blot experiments. S.L., J.K. and K.M.M. performed and quantified IF
614 data. M.T. and S.M. conducted DRIP-seq and ChIP-seq data analysis. C.B. performed
615 DRIP-qPCR validations and HeLa R-loop IP. B.S. assisted with cell culture experiments
616 and R-loop quantification. M.R.B. assisted with cell culture studies. M.C.J., N.A.T.,
617 D.J.S., E.N.B. and L.B.A. performed bioinformatic analyses. M.A.C. contributed
618 biochemical experiments. R.S.H. and J.L.M. drafted the manuscript with input from all
619 other authors.

620

621 **Competing interest statement**

622 The authors have no conflicts to declare.

623

624 **References**

- 625 1. Green, A.M. & Weitzman, M.D. The spectrum of APOBEC3 activity: from anti-viral
626 agents to anti-cancer opportunities. *DNA Repair (Amst)* **83**, 102700 (2019).
- 627 2. Harris, R.S. & Dudley, J.P. APOBECs and virus restriction. *Virology* **479-480**, 131-45
628 (2015).
- 629 3. Sheehy, A.M., Gaddis, N.C., Choi, J.D. & Malim, M.H. Isolation of a human gene that
630 inhibits HIV-1 infection and is suppressed by the viral Vif protein. *Nature* **418**,
631 646-50 (2002).
- 632 4. Harris, R.S. *et al.* DNA deamination mediates innate immunity to retroviral infection.
633 *Cell* **113**, 803-9 (2003).

- 634 5. Zhang, H. *et al.* The cytidine deaminase CEM15 induces hypermutation in newly
635 synthesized HIV-1 DNA. *Nature* **424**, 94-8 (2003).
- 636 6. Mangeat, B. *et al.* Broad antiretroviral defence by human APOBEC3G through lethal
637 editing of nascent reverse transcripts. *Nature* **424**, 99-103 (2003).
- 638 7. Shi, K. *et al.* Structural basis for targeted DNA cytosine deamination and
639 mutagenesis by APOBEC3A and APOBEC3B. *Nat Struct Mol Biol* **24**, 131-139
640 (2017).
- 641 8. Kohli, R.M. *et al.* Local sequence targeting in the AID/APOBEC family differentially
642 impacts retroviral restriction and antibody diversification. *J Biol Chem* **285**,
643 40956-64 (2010).
- 644 9. Rathore, A. *et al.* The local dinucleotide preference of APOBEC3G can be altered
645 from 5'-CC to 5'-TC by a single amino acid substitution. *J Mol Biol* **425**, 4442-54
646 (2013).
- 647 10. Wang, M., Rada, C. & Neuberger, M.S. Altering the spectrum of immunoglobulin V
648 gene somatic hypermutation by modifying the active site of AID. *J Exp Med* **207**,
649 141-53 (2010).
- 650 11. Carpenter, M.A., Rajagurubandara, E., Wijesinghe, P. & Bhagwat, A.S.
651 Determinants of sequence-specificity within human AID and APOBEC3G. *DNA*
652 *Repair (Amst)* **9**, 579-87 (2010).
- 653 12. Swanton, C., McGranahan, N., Starrett, G.J. & Harris, R.S. APOBEC enzymes:
654 mutagenic fuel for cancer evolution and heterogeneity. *Cancer Discov* **5**, 704-12
655 (2015).

- 656 13. Siriwardena, S.U., Chen, K. & Bhagwat, A.S. Functions and malfunctions of
657 mammalian DNA-cytosine deaminases. *Chem Rev* **116**, 12688-12710 (2016).
- 658 14. Venkatesan, S. *et al.* Perspective: APOBEC mutagenesis in drug resistance and
659 immune escape in HIV and cancer evolution. *Ann Oncol* **29**, 563-572 (2018).
- 660 15. Roberts, S.A. & Gordenin, D.A. Hypermutation in human cancer genomes: footprints
661 and mechanisms. *Nat Rev Cancer* **14**, 786-800 (2014).
- 662 16. Helleday, T., Eshtad, S. & Nik-Zainal, S. Mechanisms underlying mutational
663 signatures in human cancers. *Nat Rev Genet* **15**, 585-98 (2014).
- 664 17. Casellas, R. *et al.* Mutations, kataegis and translocations in B cells: understanding
665 AID promiscuous activity. *Nat Rev Immunol* **16**, 164-76 (2016).
- 666 18. Basso, K. & Dalla-Favera, R. Germinal centres and B cell lymphomagenesis. *Nat*
667 *Rev Immunol* **15**, 172-84 (2015).
- 668 19. Liu, M. *et al.* Two levels of protection for the B cell genome during somatic
669 hypermutation. *Nature* **451**, 841-5 (2008).
- 670 20. Alexandrov, L.B. *et al.* The repertoire of mutational signatures in human cancer.
671 *Nature* **578**, 94-101 (2020).
- 672 21. Burns, M.B., Temiz, N.A. & Harris, R.S. Evidence for APOBEC3B mutagenesis in
673 multiple human cancers. *Nat Genet* **45**, 977-83 (2013).
- 674 22. Burns, M.B. *et al.* APOBEC3B is an enzymatic source of mutation in breast cancer.
675 *Nature* **494**, 366-70 (2013).
- 676 23. Roberts, S.A. *et al.* An APOBEC cytidine deaminase mutagenesis pattern is
677 widespread in human cancers. *Nat Genet* **45**, 970-6 (2013).

- 678 24. Alexandrov, L.B. *et al.* Signatures of mutational processes in human cancer. *Nature*
679 **500**, 415-21 (2013).
- 680 25. Nik-Zainal, S. *et al.* Mutational processes molding the genomes of 21 breast
681 cancers. *Cell* **149**, 979-93 (2012).
- 682 26. Chan, K. *et al.* An APOBEC3A hypermutation signature is distinguishable from the
683 signature of background mutagenesis by APOBEC3B in human cancers. *Nat*
684 *Genet* **47**, 1067-72 (2015).
- 685 27. Nik-Zainal, S. *et al.* Association of a germline copy number polymorphism of
686 APOBEC3A and APOBEC3B with burden of putative APOBEC-dependent
687 mutations in breast cancer. *Nat Genet* **46**, 487-91 (2014).
- 688 28. Cortez, L.M. *et al.* APOBEC3A is a prominent cytidine deaminase in breast cancer.
689 *PLoS Genet* **15**, e1008545 (2019).
- 690 29. Seplyarskiy, V.B. *et al.* APOBEC-induced mutations in human cancers are strongly
691 enriched on the lagging DNA strand during replication. *Genome Res* **26**, 174-82
692 (2016).
- 693 30. Hoopes, J.I. *et al.* APOBEC3A and APOBEC3B preferentially deaminates the
694 lagging strand template during DNA replication. *Cell Rep* **14**, 1273-1282 (2016).
- 695 31. Bhagwat, A.S. *et al.* Strand-biased cytosine deamination at the replication fork
696 causes cytosine to thymine mutations in *Escherichia coli*. *Proc Natl Acad Sci U S*
697 *A* **113**, 2176-81 (2016).
- 698 32. Haradhvala, N.J. *et al.* Mutational strand asymmetries in cancer genomes reveal
699 mechanisms of DNA damage and repair. *Cell* **164**, 538-49 (2016).

- 700 33. Morganella, S. *et al.* The topography of mutational processes in breast cancer
701 genomes. *Nat Commun* **7**, 11383 (2016).
- 702 34. Sui, Y. *et al.* Analysis of APOBEC-induced mutations in yeast strains with low levels
703 of replicative DNA polymerases. *Proc Natl Acad Sci U S A* **117**, 9440-9450
704 (2020).
- 705 35. Nik-Zainal, S. *et al.* Landscape of somatic mutations in 560 breast cancer whole-
706 genome sequences. *Nature* **534**, 47-54 (2016).
- 707 36. Buisson, R. *et al.* Passenger hotspot mutations in cancer driven by APOBEC3A and
708 mesoscale genomic features. *Science* **364**(2019).
- 709 37. Taylor, B.J. *et al.* DNA deaminases induce break-associated mutation showers with
710 implication of APOBEC3B and 3A in breast cancer kataegis. *Elife* **2**, e00534
711 (2013).
- 712 38. García-Muse, T. & Aguilera, A. R Loops: from physiological to pathological roles.
713 *Cell* **179**, 604-618 (2019).
- 714 39. Crossley, M.P., Bocek, M. & Cimprich, K.A. R-Loops as cellular regulators and
715 genomic threats. *Mol Cell* **73**, 398-411 (2019).
- 716 40. Belotserkovskii, B.P., Tornaletti, S., D'Souza, A.D. & Hanawalt, P.C. R-loop
717 generation during transcription: Formation, processing and cellular outcomes.
718 *DNA Repair (Amst)* **71**, 69-81 (2018).
- 719 41. Zanotti, K.J. & Gearhart, P.J. Antibody diversification caused by disrupted mismatch
720 repair and promiscuous DNA polymerases. *DNA Repair (Amst)* **38**, 110-116
721 (2016).

- 722 42. Pilzecker, B. & Jacobs, H. Mutating for good: DNA damage responses during
723 somatic hypermutation. *Front Immunol* **10**, 438 (2019).
- 724 43. Hamperl, S., Bocek, M.J., Saldivar, J.C., Swigut, T. & Cimprich, K.A. Transcription-
725 replication conflict orientation modulates R-Loop levels and activates distinct
726 DNA damage responses. *Cell* **170**, 774-786.e19 (2017).
- 727 44. Kim, J.J. *et al.* Systematic bromodomain protein screens identify homologous
728 recombination and R-loop suppression pathways involved in genome integrity.
729 *Genes Dev* **33**, 1751-1774 (2019).
- 730 45. Bayona-Feliu, A., Barroso, S., Muñoz, S. & Aguilera, A. The SWI/SNF chromatin
731 remodeling complex helps resolve R-loop-mediated transcription-replication
732 conflicts. *Nat Genet* **53**, 1050-1063 (2021).
- 733 46. Sollier, J. & Cimprich, K.A. Breaking bad: R-loops and genome integrity. *Trends Cell*
734 *Biol* **25**, 514-22 (2015).
- 735 47. Aguilera, A. & García-Muse, T. R loops: from transcription byproducts to threats to
736 genome stability. *Mol Cell* **46**, 115-24 (2012).
- 737 48. Skourti-Stathaki, K. & Proudfoot, N.J. A double-edged sword: R loops as threats to
738 genome integrity and powerful regulators of gene expression. *Genes Dev* **28**,
739 1384-96 (2014).
- 740 49. Richard, P. & Manley, J.L. R Loops and links to human disease. *J Mol Biol* **429**,
741 3168-3180 (2017).
- 742 50. Groh, M. & Gromak, N. Out of balance: R-loops in human disease. *PLoS Genet* **10**,
743 e1004630 (2014).

- 744 51. Wells, J.P., White, J. & Stirling, P.C. R Loops and their composite cancer
745 connections. *Trends Cancer* **5**, 619-631 (2019).
- 746 52. Serebrenik, A.A. *et al.* The deaminase APOBEC3B triggers the death of cells
747 lacking uracil DNA glycosylase. *Proc Natl Acad Sci U S A* **116**, 22158-22163
748 (2019).
- 749 53. Cristini, A., Groh, M., Kristiansen, M.S. & Gromak, N. RNA/DNA hybrid interactome
750 identifies DXH9 as a molecular player in transcriptional termination and R-Loop-
751 associated DNA damage. *Cell Rep* **23**, 1891-1905 (2018).
- 752 54. McCann, J.L. *et al.* The DNA deaminase APOBEC3B interacts with the cell-cycle
753 protein CDK4 and disrupts CDK4-mediated nuclear import of Cyclin D1. *J Biol*
754 *Chem* **294**, 12099-12111 (2019).
- 755 55. McCann, J.L., Salamango, D.J., Law, E.K., Brown, W.L. & Harris, R.S. MagnEdit-
756 interacting factors that recruit DNA-editing enzymes to single base targets. *Life*
757 *Sci Alliance* **3**, e201900606 (2020).
- 758 56. Boguslawski, S.J. *et al.* Characterization of monoclonal antibody to DNA:RNA and
759 its application to immunodetection of hybrids. *J Immunol Methods* **89**, 123-30
760 (1986).
- 761 57. Phillips, D.D. *et al.* The sub-nanomolar binding of DNA-RNA hybrids by the single-
762 chain Fv fragment of antibody S9.6. *J Mol Recognit* **26**, 376-81 (2013).
- 763 58. Leonard, B. *et al.* The PKC/NF- κ B signaling pathway induces APOBEC3B
764 expression in multiple human cancers. *Cancer Res* **75**, 4538-47 (2015).

- 765 59. El Hage, A., French, S.L., Beyer, A.L. & Tollervey, D. Loss of Topoisomerase I leads
766 to R-loop-mediated transcriptional blocks during ribosomal RNA synthesis.
767 *Genes Dev* **24**, 1546-58 (2010).
- 768 60. Tuduri, S. *et al.* Topoisomerase I suppresses genomic instability by preventing
769 interference between replication and transcription. *Nat Cell Biol* **11**, 1315-24
770 (2009).
- 771 61. Smolka, J.A., Sanz, L.A., Hartono, S.R. & Chédin, F. Recognition of RNA by the
772 S9.6 antibody creates pervasive artifacts when imaging RNA:DNA hybrids. *J Cell*
773 *Biol* **220**, e202004079 (2021).
- 774 62. Cheng, A.Z. *et al.* Epstein-Barr virus BORF2 inhibits cellular APOBEC3B to
775 preserve viral genome integrity. *Nat Microbiol* **4**, 78-88 (2019).
- 776 63. Jarvis, M.C., Ebrahimi, D., Temiz, N.A. & Harris, R.S. Mutation signatures including
777 APOBEC in cancer cell lines. *JNCI Cancer Spectr* **2**, pky002 (2018).
- 778 64. Leonard, B. *et al.* APOBEC3B upregulation and genomic mutation patterns in
779 serous ovarian carcinoma. *Cancer Res* **73**, 7222-31 (2013).
- 780 65. Edwards, D.S. *et al.* BRD4 prevents R-Loop formation and transcription-replication
781 conflicts by ensuring efficient transcription elongation. *Cell Rep* **32**, 108166
782 (2020).
- 783 66. Lam, F.C. *et al.* BRD4 prevents the accumulation of R-loops and protects against
784 transcription-replication collision events and DNA damage. *Nat Commun* **11**,
785 4083 (2020).

- 786 67. Ito, F., Fu, Y., Kao, S.A., Yang, H. & Chen, X.S. Family-wide comparative analysis
787 of cytidine and methylcytidine deamination by eleven human APOBEC proteins.
788 *J Mol Biol* **429**, 1787-1799 (2017).
- 789 68. Adolph, M.B., Love, R.P., Feng, Y. & Chelico, L. Enzyme cycling contributes to
790 efficient induction of genome mutagenesis by the cytidine deaminase
791 APOBEC3B. *Nucleic Acids Res* **45**, 11925-11940 (2017).
- 792 69. DeNizio, J.E., Schutsky, E.K., Berrios, K.N., Liu, M.Y. & Kohli, R.M. Harnessing
793 natural DNA modifying activities for editing of the genome and epigenome. *Curr*
794 *Opin Chem Biol* **45**, 10-17 (2018).
- 795 70. Olson, M.E., Harris, R.S. & Harki, D.A. APOBEC enzymes as targets for virus and
796 cancer therapy. *Cell Chem Biol* **25**, 36-49 (2018).
- 797 71. Chaurasiya, K.R. *et al.* Oligomerization transforms human APOBEC3G from an
798 efficient enzyme to a slowly dissociating nucleic acid-binding protein. *Nat Chem*
799 **6**, 28-33 (2014).
- 800 72. Ara, A., Love, R.P. & Chelico, L. Different mutagenic potential of HIV-1 restriction
801 factors APOBEC3G and APOBEC3F is determined by distinct single-stranded
802 DNA scanning mechanisms. *PLoS Pathog* **10**, e1004024 (2014).
- 803 73. Chelico, L., Prochnow, C., Erie, D.A., Chen, X.S. & Goodman, M.F. Structural model
804 for deoxycytidine deamination mechanisms of the HIV-1 inactivation enzyme
805 APOBEC3G. *J Biol Chem* **285**, 16195-205 (2010).
- 806 74. Bennett, R.P., Salter, J.D., Liu, X., Wedekind, J.E. & Smith, H.C. APOBEC3G
807 subunits self-associate via the C-terminal deaminase domain. *J Biol Chem* **283**,
808 33329-36 (2008).

- 809 75. Li, J. *et al.* APOBEC3 multimerization correlates with HIV-1 packaging and
810 restriction activity in living cells. *J Mol Biol* **426**, 1296-307 (2014).
- 811 76. Allison, D.F. & Wang, G.G. R-loops: formation, function, and relevance to cell
812 stress. *Cell Stress* **3**, 38-46 (2019).
- 813 77. Bensaude, O. Inhibiting eukaryotic transcription: Which compound to choose? How
814 to evaluate its activity? *Transcription* **2**, 103-108 (2011).
- 815 78. Wang, Y., Lu, J.J., He, L. & Yu, Q. Triptolide (TPL) inhibits global transcription by
816 inducing proteasome-dependent degradation of RNA polymerase II (Pol II). *PLoS*
817 *One* **6**, e23993 (2011).
- 818 79. Sanz, L.A. *et al.* Prevalent, dynamic, and conserved R-Loop structures associate
819 with specific epigenomic signatures in mammals. *Mol Cell* **63**, 167-78 (2016).
- 820 80. Manzo, S.G. *et al.* DNA Topoisomerase I differentially modulates R-loops across the
821 human genome. *Genome Biol* **19**, 100 (2018).
- 822 81. Nojima, T. *et al.* Deregulated expression of mammalian lncRNA through loss of
823 SPT6 induces R-Loop formation, replication stress, and cellular senescence. *Mol*
824 *Cell* **72**, 970-984.e7 (2018).
- 825 82. Kotsantis, P. *et al.* Increased global transcription activity as a mechanism of
826 replication stress in cancer. *Nat Commun* **7**, 13087 (2016).
- 827 83. Stork, C.T. *et al.* Co-transcriptional R-loops are the main cause of estrogen-induced
828 DNA damage. *Elife* **5**, e17548 (2016).
- 829 84. Holden, N.S. *et al.* Phorbol ester-stimulated NF- κ B-dependent transcription: roles for
830 isoforms of novel protein kinase C. *Cell Signal* **20**, 1338-48 (2008).

- 831 85. Xiao, X. *et al.* Structural determinants of APOBEC3B non-catalytic domain for
832 molecular assembly and catalytic regulation. *Nucleic Acids Res* **45**, 7540 (2017).
- 833 86. Salamango, D.J. *et al.* APOBEC3B nuclear localization requires two distinct N-
834 terminal domain surfaces. *J Mol Biol* **430**, 2695-2708 (2018).
- 835 87. Hou, S. *et al.* Structural Analysis of the Active Site and DNA Binding of Human
836 Cytidine Deaminase APOBEC3B. *J Chem Theory Comput* **15**, 637-647 (2019).
- 837 88. Shi, K. *et al.* Active site plasticity and possible modes of chemical inhibition of the
838 human DNA deaminase APOBEC3B. *FASEB Bioadv* **2**, 49-58 (2020).
- 839 89. Law, E.K. *et al.* APOBEC3A catalyzes mutation and drives carcinogenesis in vivo. *J*
840 *Exp Med* **217**(2020).
- 841 90. Li, X. & Manley, J.L. Inactivation of the SR protein splicing factor ASF/SF2 results in
842 genomic instability. *Cell* **122**, 365-78 (2005).
- 843 91. Chen, L. *et al.* The augmented R-Loop is a unifying mechanism for myelodysplastic
844 syndromes induced by high-risk splicing factor mutations. *Mol Cell* **69**, 412-
845 425.e6 (2018).
- 846 92. Wan, Y. *et al.* Splicing function of mitotic regulators links R-loop-mediated DNA
847 damage to tumor cell killing. *J Cell Biol* **209**, 235-46 (2015).
- 848 93. ICGC/TCGA. Pan-cancer analysis of whole genomes. *Nature* **578**, 82-93 (2020).
- 849 94. Villarreal, O.D., Mersaoui, S.Y., Yu, Z., Masson, J.Y. & Richard, S. Genome-wide R-
850 loop analysis defines unique roles for DDX5, XRN2, and PRMT5 in DNA/RNA
851 hybrid resolution. *Life Sci Alliance* **3**, e202000762 (2020).

- 852 95. Pérez-Calero, C. *et al.* UAP56/DDX39B is a major cotranscriptional RNA-DNA
853 helicase that unwinds harmful R loops genome-wide. *Genes Dev* **34**, 898-912
854 (2020).
- 855 96. Cohen, S. *et al.* Senataxin resolves RNA:DNA hybrids forming at DNA double-
856 strand breaks to prevent translocations. *Nat Commun* **9**, 533 (2018).
- 857 97. Skourti-Stathaki, K., Proudfoot, N.J. & Gromak, N. Human senataxin resolves
858 RNA/DNA hybrids formed at transcriptional pause sites to promote Xrn2-
859 dependent termination. *Mol Cell* **42**, 794-805 (2011).
- 860 98. Sollier, J. *et al.* Transcription-coupled nucleotide excision repair factors promote R-
861 loop-induced genome instability. *Mol Cell* **56**, 777-85 (2014).
- 862 99. Bhatia, V. *et al.* BRCA2 prevents R-loop accumulation and associates with TREX-2
863 mRNA export factor PCID2. *Nature* **511**, 362-5 (2014).
- 864 100. Shivji, M.K.K., Renaudin, X., Williams, Ç. & Venkitaraman, A.R. BRCA2 regulates
865 transcription elongation by RNA Polymerase II to prevent R-Loop accumulation.
866 *Cell Rep* **22**, 1031-1039 (2018).
- 867 101. Chen, L. *et al.* R-ChIP using inactive RNase H reveals dynamic coupling of R-
868 loops with transcriptional pausing at gene promoters. *Mol Cell* **68**, 745-757.e5
869 (2017).
- 870 102. Hatchi, E. *et al.* BRCA1 recruitment to transcriptional pause sites is required for R-
871 loop-driven DNA damage repair. *Mol Cell* **57**, 636-647 (2015).
- 872 103. Liang, Z. *et al.* Binding of FANCI-FANCD2 complex to RNA and R-Loops
873 stimulates robust FANCD2 monoubiquitination. *Cell Rep* **26**, 564-572.e5 (2019).

- 874 104. Gu, S., Bodai, Z., Cowan, Q.T. & Komor, A.C. Base editors: Expanding the types
875 of DNA damage products harnessed for genome editing. *Gene Genome Ed*
876 **1**(2021).
- 877 105. Morales, J.C. *et al.* XRN2 links transcription termination to DNA damage and
878 replication stress. *PLoS Genet* **12**, e1006107 (2016).
- 879 106. Mersaoui, S.Y. *et al.* Arginine methylation of the DDX5 helicase RGG/RG motif by
880 PRMT5 regulates resolution of RNA:DNA hybrids. *EMBO J* **38**, e100986 (2019).
- 881 107. Nikkila, J. *et al.* Elevated APOBEC3B expression drives a kataegic-like mutation
882 signature and replication stress-related therapeutic vulnerabilities in p53-
883 defective cells. *Br J Cancer* **117**, 113-123 (2017).
- 884 108. Tellier, M., Maudlin, I. & Murphy, S. Transcription and splicing: A two-way street.
885 *Wiley Interdiscip Rev RNA* **11**, e1593 (2020).
- 886 109. Zhang, J. *et al.* Disease-causing mutations in SF3B1 alter splicing by disrupting
887 interaction with SUGP1. *Mol Cell* **76**, 82-95.e7 (2019).
- 888 110. Chervova, A. *et al.* Analysis of gene expression and mutation data points on
889 contribution of transcription to the mutagenesis by APOBEC enzymes. *NAR*
890 *Cancer* **3**, zcab025 (2021).
- 891 111. Mas-Ponte, D. & Supek, F. DNA mismatch repair promotes APOBEC3-mediated
892 diffuse hypermutation in human cancers. *Nat Genet* **52**, 958-968 (2020).
- 893 112. García-Rubio, M.L. *et al.* The Fanconi anemia pathway protects genome integrity
894 from R-loops. *PLoS Genet* **11**, e1005674 (2015).
- 895 113. Schwab, R.A. *et al.* The Fanconi anemia pathway maintains genome stability by
896 coordinating replication and transcription. *Mol Cell* **60**, 351-61 (2015).

- 897 114. Periyasamy, M. *et al.* Induction of APOBEC3B expression by chemotherapy drugs
898 is mediated by DNA-PK-directed activation of NF- κ B. *Oncogene* **40**, 1077-1090
899 (2021).
- 900 115. Roelofs, P.A. *et al.* Characterization of the mechanism by which the RB/E2F
901 pathway controls expression of the cancer genomic DNA deaminase
902 APOBEC3B. *Elife* **9**(2020).
- 903 116. Hamperl, S. & Cimprich, K.A. The contribution of co-transcriptional RNA:DNA
904 hybrid structures to DNA damage and genome instability. *DNA Repair (Amst)* **19**,
905 84-94 (2014).
- 906 117. Chen, Y. *et al.* DHX9 interacts with APOBEC3B and attenuates the anti-HBV effect
907 of APOBEC3B. *Emerg Microbes Infect* **9**, 366-377 (2020).
- 908
- 909

910 **Figure legends**

911

912 **Fig. 1. A3B interacts with R-loop-associated proteins**

913 **a**, Information on shared proteins between A3B and S9.6 AP-MS datasets.

914 **b**, Pie chart depicting overlap between A3B and S9.6 AP-MS datasets.

915 **c**, Immunoblot and IF microscopy analysis of MCF10A-TREx-A3B-eGFP cells treated
916 with vehicle or Dox (1 $\mu\text{g}/\text{mL}$, 24 hrs). Nuclear A3B-eGFP is green and nuclear DNA is
917 blue (DAPI; representative images; 10 μm scale bar).

918 **d**, Immunoblots of A3B-eGFP or IgG IP from TREx-A3B-eGFP MCF10A cells +/- Dox (1
919 $\mu\text{g}/\text{ml}$, 24 hrs), treated with PMA (25 ng/ml, 2 hrs), and probed with indicated antibodies
920 (upper images). Slot blot of A3B-eGFP IP from TREx-A3B-eGFP MCF10A cells +/- Dox
921 (1 $\mu\text{g}/\text{ml}$, 24 hrs) probed with S9.6 antibody (lower images). RNase H (RNH) treatment
922 confirmed specificity of R-loop signal.

923 **e**, Immunoblots of the indicated proteins in input lysates and S9.6 IP reactions from
924 MCF10A (WT) or A3B-null derivatives (KO) treated with PMA (25 ng/ml, 5 hrs). R-loop
925 specificity is indicated by signal depletion by RNA/DNA hybrid competitor.

926

927 **Fig. 2. Elevated nuclear R-loop levels in A3B-null and A3B-depleted cells**

928 **a-b**, IF images and quantification of MCF10A (WT) and A3B-null (KO) cells stained with
929 S9.6 (green) and DAPI (blue). Diminution of nucleoplasmic S9.6 signal by exogenous
930 RNase H (RNH) confirmed signal specificity (representative images; 5 μm scale bar; $n >$
931 100 nuclei per condition; red bars represent mean \pm SEM; ****, $P < 0.0001$ by Mann-

932 Whitney test).

933 **c-d**, S9.6 dot blot analysis of a MCF10A (WT) and *A3B*-null (KO) genomic DNA dilution
934 series +/- exogenous RNase H (RNH; representative images). Parallel dsDNA dot blots
935 provided a loading control. Quantification normalized to the most concentrated WT
936 signal ($n \geq 4$; mean \pm SEM; *, $P < 0.05$ by two-tailed unpaired t-test).

937 **e-f**, IF images and quantification of U2OS shCtrl and shA3B cells stained with S9.6
938 (green) and DAPI (blue). Diminution of nucleoplasmic S9.6 signal by exogenous RNase
939 H (RNH) confirmed signal specificity (representative images; 5 μ m scale bar; $n > 100$
940 nuclei per condition; red bars represent mean \pm SEM; ****, $P < 0.0001$ by Mann-Whitney
941 test).

942 **g-h**, S9.6 dot blot analysis of a U2OS shCtrl and shA3B genomic DNA dilution series +/-
943 exogenous RNase H (RNH; representative images). Parallel dsDNA dot blots provided
944 a loading control. Quantification normalized to the most concentrated shCtrl signal ($n \geq$
945 4; mean \pm SEM; ***, $P < 0.001$ by two-tailed unpaired t-test).

946 **i-j**, IF images and quantification of MCF10A (WT) and *A3B*-null (KO) cells stained with
947 S9.6 (green), DAPI (blue), and γ -H2AX (representative images; 5 μ m scale bar; $n > 100$
948 nuclei per condition; red bars represent mean \pm SEM; ****, $P < 0.0001$ by Mann-Whitney
949 test, ***, $P < 0.001$ by two-tailed unpaired t-test).

950 **k-l**, IF images and quantification of U2OS shCtrl and shA3B cells stained with S9.6
951 (green), DAPI (blue), and γ -H2AX (representative images; 5 μ m scale bar; $n > 100$
952 nuclei per condition; red bars represent mean \pm SEM; ****, $P < 0.0001$ by Mann-Whitney
953 test, ***, $P < 0.001$ by two-tailed unpaired t-test).

954

955 **Fig. 3. A3B overexpression reduces nuclear R-loop levels**

956 **a-d**, IF images (a and c) and quantification (b and d) of U2OS cells expressing the
957 denoted eGFP construct (green) and stained with S9.6 (red) and DAPI (blue). Upper
958 panel shows experimental workflow and lower panel representative images (5 μ m scale
959 bar; n > 60 nuclei per condition; red bars represent mean \pm SEM; *, $P < 0.05$ and ***, P
960 < 0.001 by one-way ANOVA; ns, not significant).

961 **e**, Immunoblots of U2OS shCtrl or shA3B cells complemented with empty vector (EV),
962 A3B-HA, or A3B-E255A-HA. The lower image shows the results of a DNA deaminase
963 activity assay with extracts from the indicated cell lines (reaction quantification below
964 with purified A3A as a positive control and reaction buffer as a negative control).

965 **f-g**, Dot blot analysis of U2OS shCtrl or shA3B cells complemented with empty vector
966 (EV), A3B-HA, or A3B-E255A-HA. A genomic DNA dilution series +/- exogenous RNase
967 H (RNH) was probed with either S9.6 antibody or dsDNA antibody as a loading control
968 (representative images). Quantification normalized to the most concentrated shCtrl
969 signal (n = 3; mean \pm SEM; *, $P < 0.05$ by two-tailed unpaired t-test; ns, not significant).

970

971 **Fig. 4. A3B-regulated R-loops are transcription-dependent**

972 **a-b**, IF images and quantification of U2OS shCtrl and shA3B cells treated with triptolide
973 (1 μ M, 4 hrs) and subsequently stained with S9.6 (green) and DAPI (blue);
974 representative images; 5 μ m scale bar; n > 130 nuclei per condition; red bars represent
975 mean \pm SEM; ***, $P < 0.001$ and ****, $P < 0.0001$ by one-way ANOVA; ns, not
976 significant).

977 **c-d**, S9.6 dot blot analysis of a genomic DNA dilution series +/- RNH from U2OS shCtrl

978 or shA3B cells treated with triptolide (TRP; 1 μ M, 4 hrs) or flavopiridol (FLV; 1 μ M, 1 hr;
979 representative images). Parallel dsDNA dot blots provided a loading control.
980 Quantification was normalized to the most concentrated shCtrl/DMSO signal (n = 3;
981 mean \pm SEM; *, $P < 0.05$; **, $P < 0.01$ by two-tailed unpaired t-test).

982

983 **Fig. 5. A3B affects a large proportion of R-loops genome-wide**

984 **a-b**, Pie graphs representing R-loop distributions in wild-type (WT) and *A3B*-null (KO)
985 MCF10A cells.

986 **c-e**, Meta-analysis of read density (FPKM) for DRIP-seq results from wild-type (WT,
987 blue) and *A3B*-null MCF10A (KO, red) partitioned into 3 groups (increased, decreased,
988 and unchanged) as described in the text. Input read densities are indicated by
989 overlapping gray lines.

990 **f-g, h-i, j-k**, DRIP-seq profiles for representative genes in each of the groups defined in
991 panel c-e. Independent quantification by DRIP-qPCR +/- RNase H (RNH) treatment
992 (striped bars) is shown in the histogram to the right (n \geq 4; means \pm SEM expressed as
993 percentage of input; *, $P < 0.05$; **, $P < 0.01$; ****, $P < 0.0001$ by two-tailed unpaired t-
994 test; ns, not significant).

995

996 **Fig. 6. Kinetics of R-loop induction and resolution**

997 **a**, Schematic of the DRIP-seq workflow used for panels d-e.

998 **b**, RT-qPCR of *A3B* mRNA from MCF10A (WT) and *A3B*-null (KO) cells treated with
999 PMA (25 ng/ml) for the indicated times. Values are expressed relative to the
1000 housekeeping gene, *TBP* (n = 3; mean \pm SEM; knockout levels not detectable).

1001 **c**, Immunoblots of extracts from MCF10A (WT) and *A3B*-null (KO) cells treated with
1002 PMA (25 ng/ml) for the indicated times and probed with indicated antibodies.

1003 **d**, DRIP-seq profiles for two PMA-responsive genes, *JUNB* and *DUSP1*, in DMSO or
1004 PMA-treated MCF10A (WT; upper profiles) and *A3B*-null (KO; lower profiles).
1005 Independent quantification by DRIP-qPCR +/- RNase H (RNH) treatment (striped bars)
1006 is shown in the histogram to the right ($n \geq 4$; mean \pm SEM normalized to DMSO WT; *,
1007 $P < 0.05$ and **, $P < 0.01$ by two-tailed unpaired t-test).

1008 **e**, DRIP-seq profiles for two PMA non-responsive genes, *GAPDH* and *HSPA8*, in
1009 DMSO or PMA-treated MCF10A (WT; upper profiles) and *A3B*-null (KO; lower profiles).
1010 Independent quantification by DRIP-qPCR +/- RNase H (RNH) treatment (striped bars)
1011 is shown in the histogram to the right ($n \geq 4$; mean \pm SEM normalized to DMSO WT; ns,
1012 not significant). *HSPA8* levels decline in WT and KO cells after PMA treatment in a
1013 manner that is independent of *A3B*.

1014 **f-g**, IF images and quantification of MCF10A (WT) and *A3B*-null (KO) cells treated with
1015 PMA for the indicated times and stained with S9.6 (green) and DAPI (blue). Diminution
1016 of nucleoplasmic S9.6 signal by exogenous RNase H (RNH) confirmed signal specificity
1017 (representative images; 5 μ m scale bar; $n > 100$ nuclei per condition; red bars represent
1018 mean \pm SEM; **, $P < 0.01$ ****, $P < 0.0001$ by Mann-Whitney test).

1019

1020 **Fig. 7. A3B biochemical activities required for R-loop resolution**

1021 **a**, Schematics of the nucleic acids used in biochemical experiments (5' fluorescent label
1022 indicated by yellow star). The 15mer short ssDNA and short RNA were used in EMSAs

1023 in panels b and f, and the 62mer long ssDNA was used alone or as annealed to the
1024 indicated complementary nucleic acids (black, DNA; red, RNA) in other experiments.

1025 **b**, Native EMSAs of A3B binding to fluorescently labeled short 15mer ssDNA or RNA in
1026 the presence of increasing concentrations of otherwise identical unlabeled competitor.
1027 The corresponding quantification shows the average fraction bound to substrate +/- SD
1028 from 3 independent experiments.

1029 **c**, Substrates in panel a tested qualitatively for deamination by A3B. Negative (-) and
1030 positive (+) controls are the long ssDNA alone and deaminated by recombinant A3A.

1031 **d**, A quantitative time course of A3B-catalyzed deamination of the long ssDNA vs an R-
1032 loop (short) substrate (mean +/- SD of n = 3 independent experiments are shown with
1033 most error bars smaller than the symbols).

1034 **e**, Subcellular localization of A3B-eGFP (WT), Mut1, and Mut2 in U2OS cells (scale bar
1035 = 10 μ M).

1036 **f**, EMSAs comparing A3B WT and Mut2 binding to short 15mer ssDNA and RNA in the
1037 presence of increasing concentrations of otherwise identical unlabeled competitor
1038 ssDNA or RNA. The corresponding quantification shows the average fraction bound to
1039 substrate +/- SD from 3 independent experiments.

1040 **g**, Quantitative comparison of A3B WT and Mut2 deamination of the long ssDNA versus
1041 an R-loop (short) substrate. Representative gels are shown for the time-dependent
1042 accumulation of product, along with quantitation of 3 independent experiments (mean
1043 +/- SD with most error bars smaller than the symbols; for comparison the WT data are
1044 the same as those in panel d).

1045 **h**, IF images and quantification of U2OS cells expressing the indicated eGFP construct

1046 (green) and stained with S9.6 (red) and DAPI (blue; 5 μ m scale bar; n > 60 nuclei per
1047 condition; red bars represent mean \pm SEM; ****, $P < 0.0001$ by one-way ANOVA; ns,
1048 not significant).

1049

1050 **Fig. 8. R-Loop mutagenesis and *kataegis* by APOBEC3B**

1051 **a**, Cartoon of a working model for A3B-mediated R-loop resolution with and without
1052 associated mutations. Other R-loop regulatory factors are depicted in shades of green
1053 and blue. Transcription, splicing, and other RNA- and R-loop-associated complexes are
1054 not shown for clarity.

1055 **b**, A dot plot showing the fraction of APOBEC3-attributed mutations (per Mbp per tumor)
1056 in the indicated overexpressed gene groups (FC, fold-change in breast tumors relative
1057 to the average observed in normal breast tissues). Pairwise comparisons are significant
1058 for all combinations of the lowest 4 versus the highest 3 expression groups ($P < 1 \times 10^{-12}$
1059 by Welsh's t-test).

1060 **c**, Stacked bar graphs showing the proportion of each COSMIC mutation signature in
1061 TCGA breast tumors with mutations in splice factor genes or not (n = 81 splice factor
1062 mutated tumors; n = 841 for non-splice factor mutated tumors; $P < 0.017$ by Fisher's
1063 exact test). The APOBEC3 signature percentage (red) is comprised of COSMIC
1064 signatures 2 and 13, and other signatures are shown in different shades of gray.

1065 **d**, Quantification of nucleoplasmic R-loop levels in U2OS cells expressing an empty
1066 vector (EV) control or A3B following a 2 hr treatment with DMSO or the splicing inhibitor
1067 Plad B (n > 50 nuclei per condition; red bars represent mean \pm SEM; ****, $P < 0.0001$ by
1068 two-tailed unpaired t-test).

1069 **e**, Distribution of the distances to the nearest SV of all non-clustered APOBEC3
1070 mutations (gold), all *kataegic* mutation events (teal), and R-loop associated APOBEC3
1071 *kataegic* mutations (red).

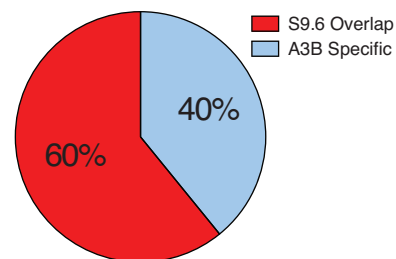
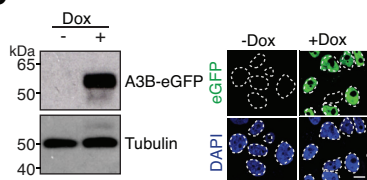
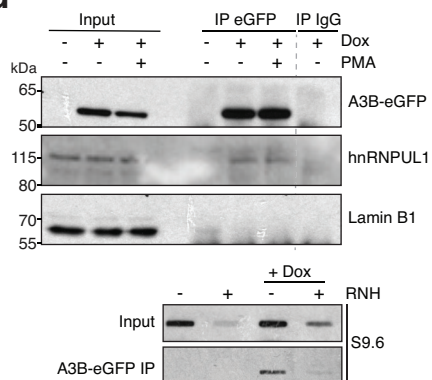
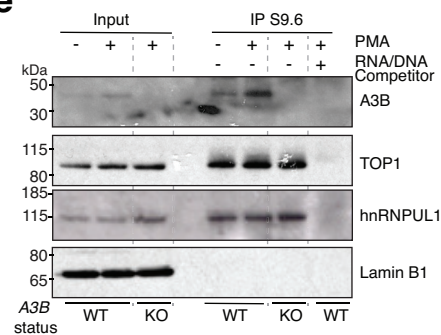
1072 **f-g**, Dot plot representations of short (≥ 3) and long (≥ 5) APOBEC3 *kataegic* tracts in
1073 PCAWG breast tumor WGS. The x- and y-axis reports A3B-associated 5'-RTCA and
1074 A3A-associated 5'-YTCA enrichments, respectively. Dashed lines indicate where non-
1075 skewed distributions should cluster, red dots represent data from specimens with at
1076 least one R-loop-associated *kataegic* event, and the gray ovals highlight the area in
1077 which 5'-RTCA enrichments occur (Mann-Whitney U-test Q-values indicated in each
1078 plot).

1079 **h**, Representative NTS *kataegic* events in the indicated genes. Wild-type trinucleotides
1080 and mutational outcomes are indicated.

1081

a

Protein Name	kDa	Accession	A3B AP-MS			S9.6 AP-MS		
			Percent Coverage	Peptides ID'd		Percent Coverage	Peptides ID'd	
				Unique	Total		Unique	Total
APOBEC3B	46	Q9UJ17	59.7	21	119	11.5	5	5
RBM8A	20	Q9Y5S9	40.2	6	20	31.0	4	4
SRSF10	31	O75494	31.7	9	28	24.0	9	9
MAP4	121	P27816	31.6	26	35	7.20	6	6
SF3B2	100	Q13435	30.8	27	47	10.5	8	8
HNRNPUL1	96	Q9BUJ2	30.5	31	79	21.4	16	16
SRSF7	27	Q16629	29.4	9	23	35.3	9	10
SNRNP200	244	O75643	24.1	40	51	17.9	30	30
MMTAG2	29	Q9BU76	24.0	5	11	34.6	7	7
RCC2	56	Q9P258	23.0	11	19	13.0	6	6
HNRNPH2	49	P55795	22.3	9	35	36.7	5	13
SKIV2L2	118	P42285	22.2	23	52	9.60	8	8
ZFR	117	Q96KR1	18.3	13	30	34.6	25	25
SAFB	103	Q15424	14.8	11	31	32.3	15	29
MOV10	114	Q9HCE1	11.2	11	19	29.6	22	22

b**c****d****e****Figure 1**

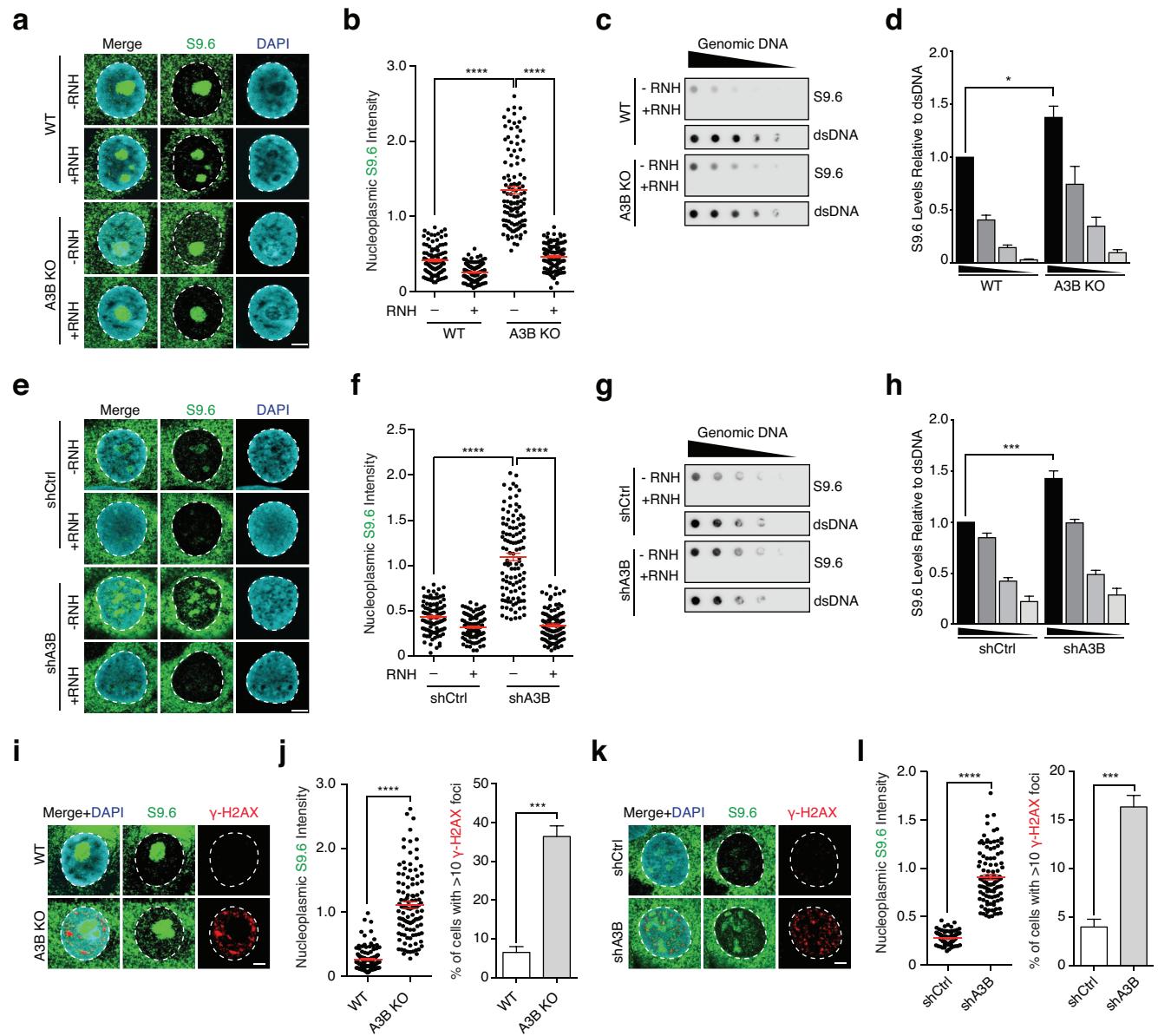
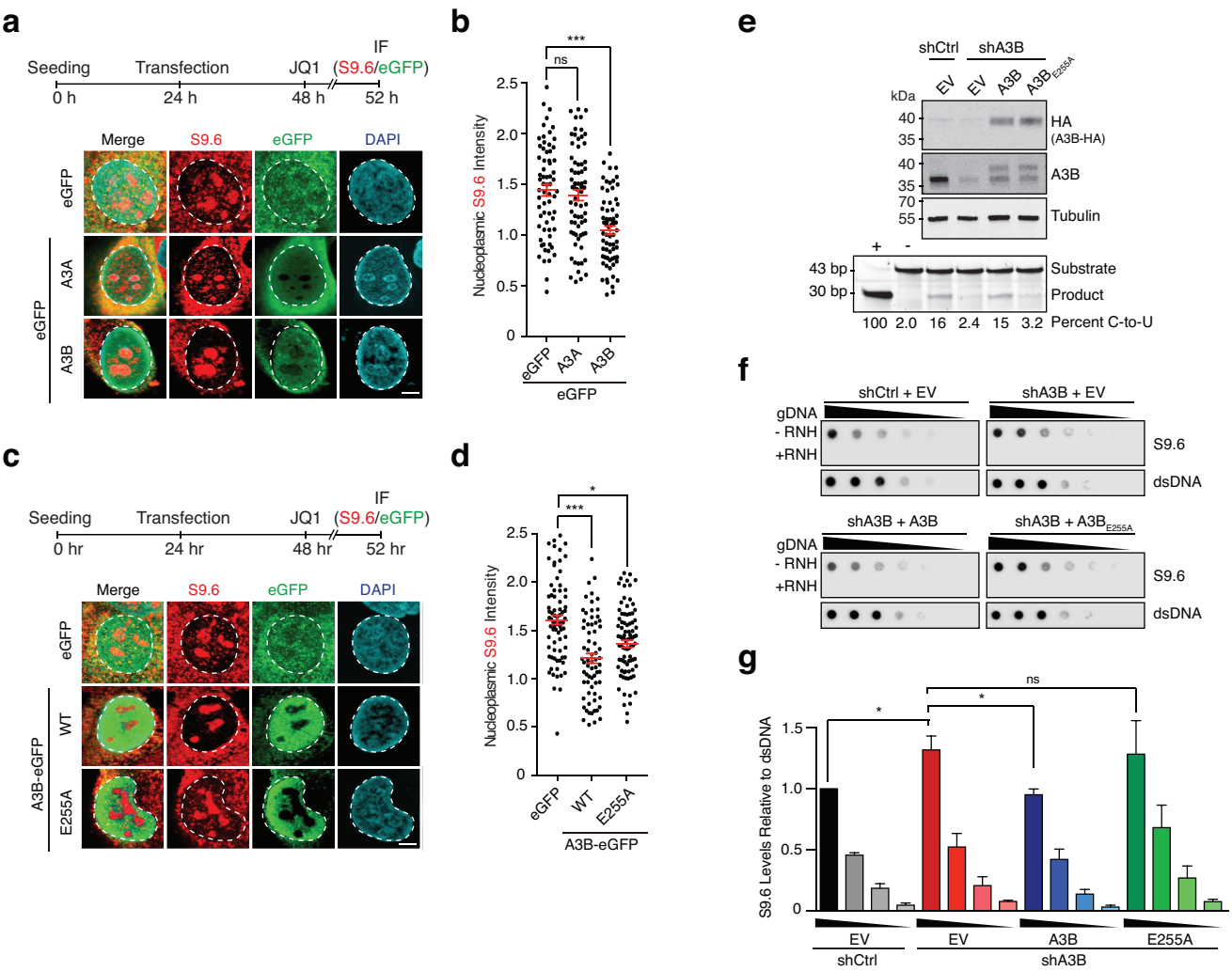


Figure 2



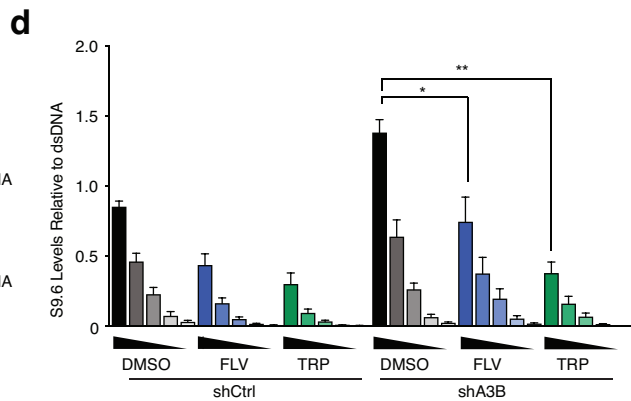
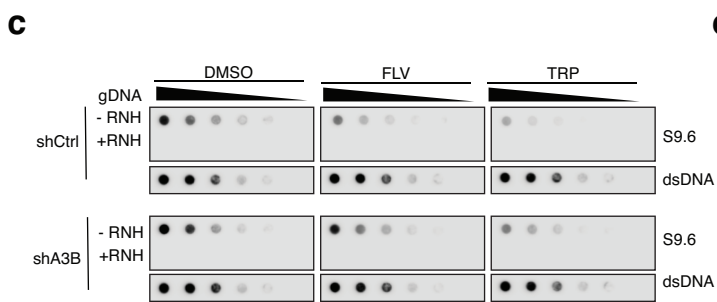
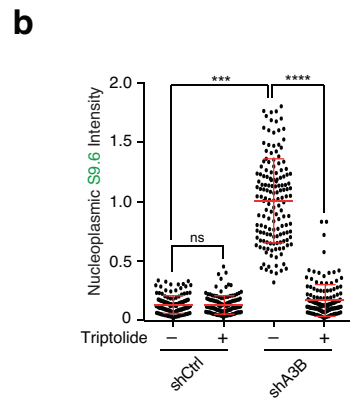
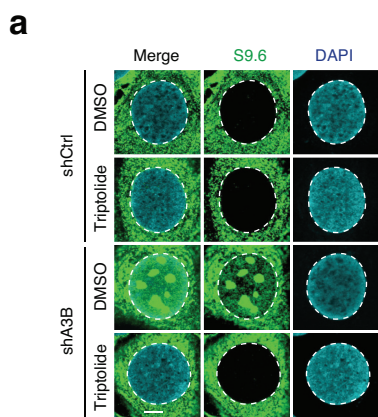


Figure 4

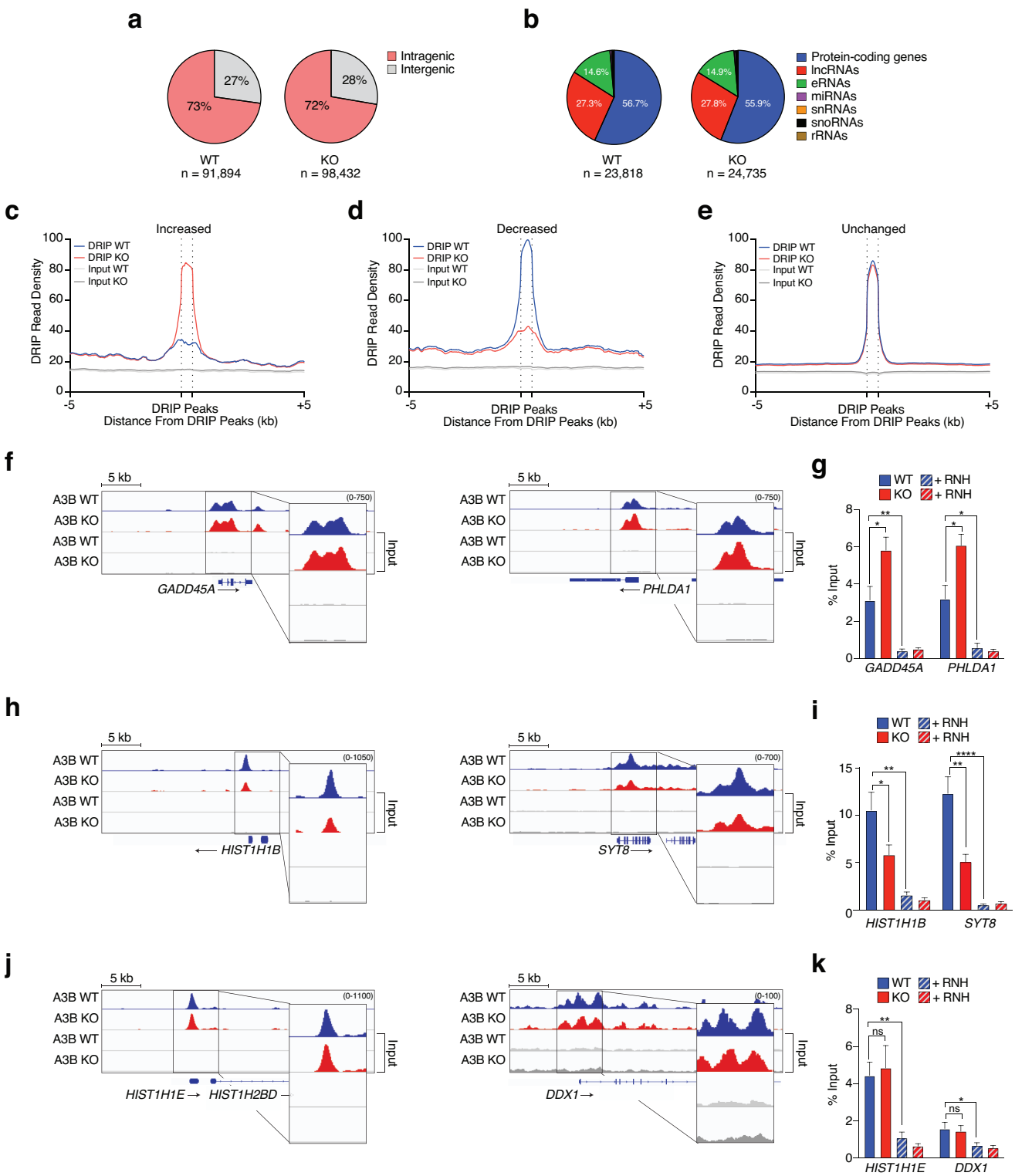


Figure 5

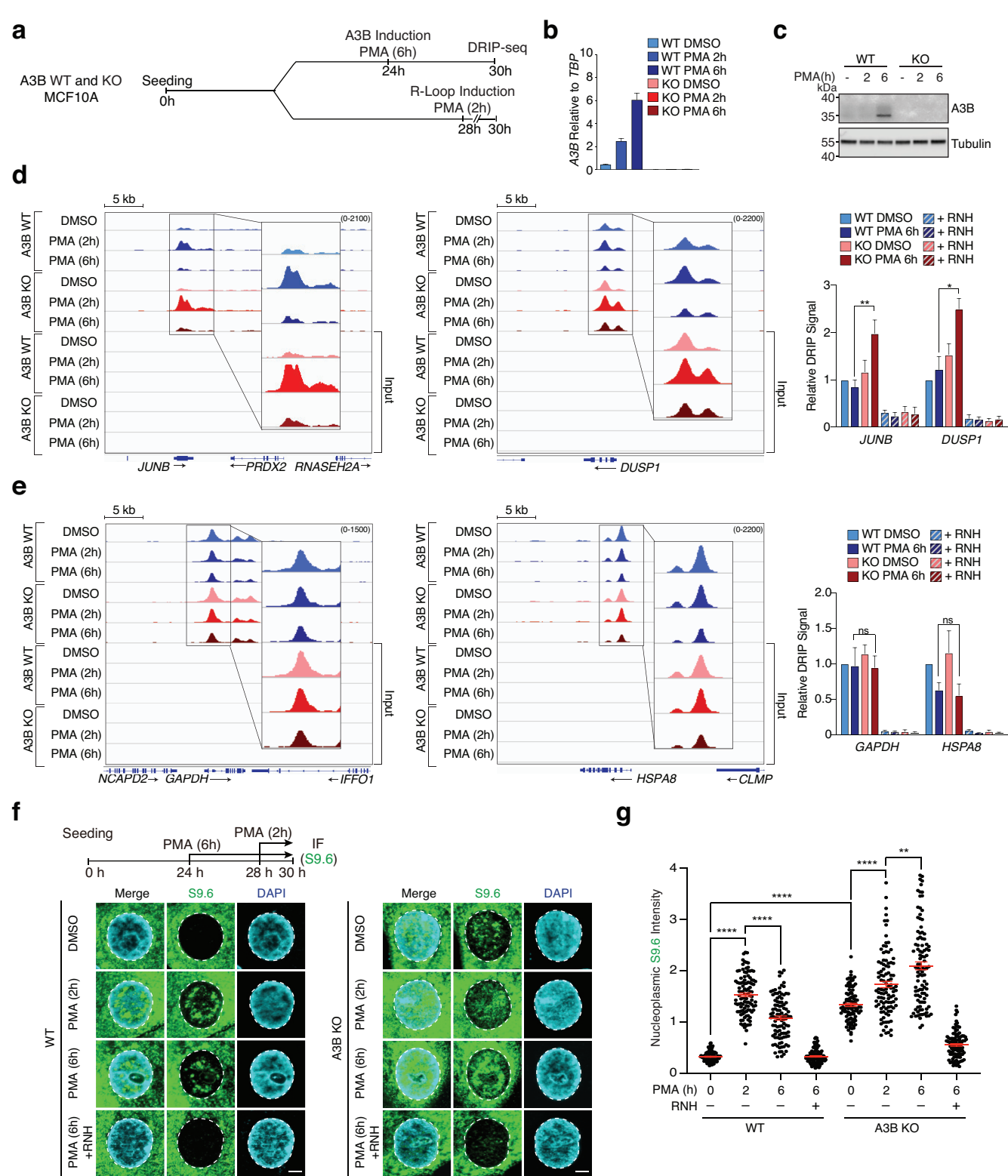


Figure 6

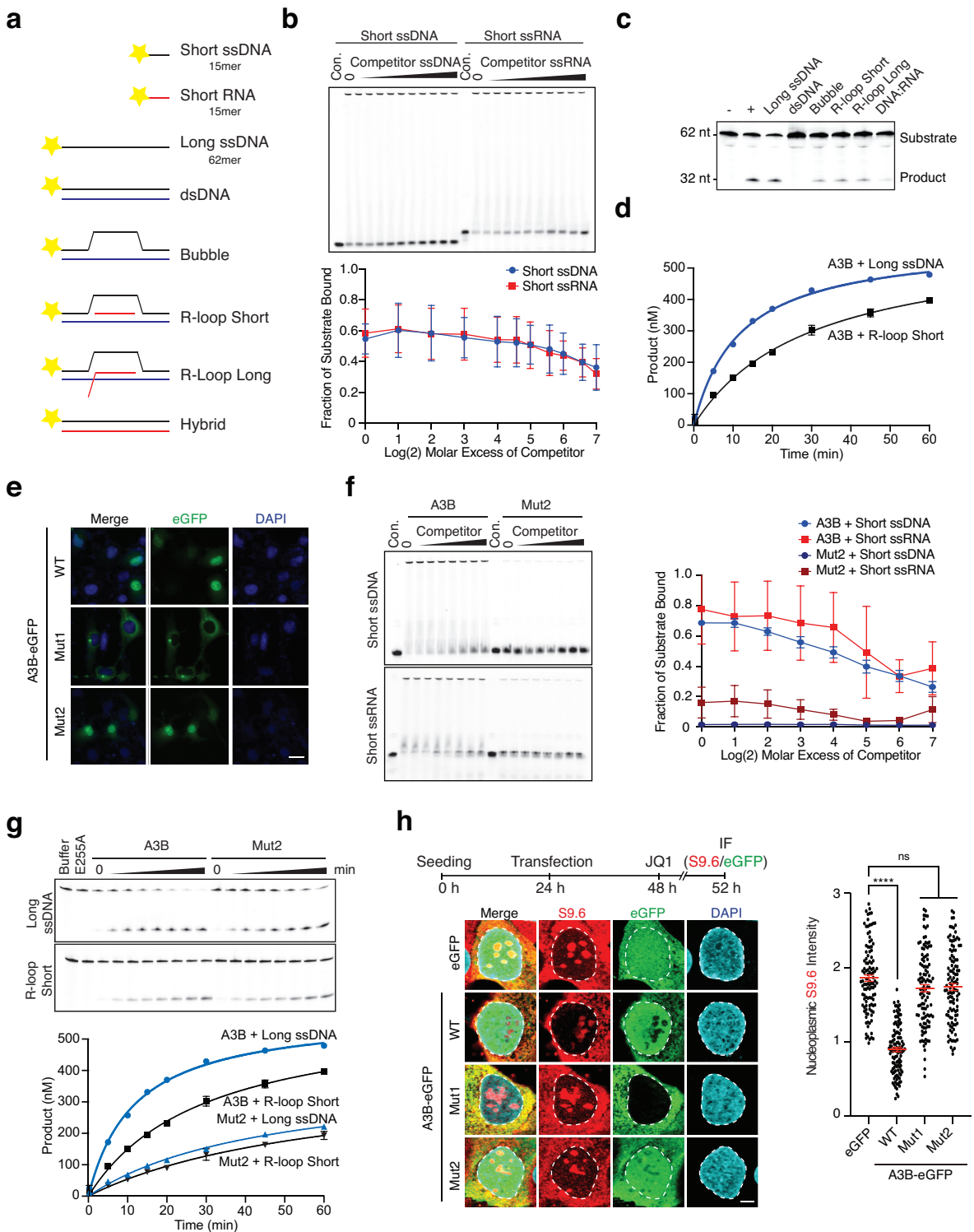


Figure 7

